[redacted]

Copy 6
RM L53D30b

NACA RM L53D30b

RESEARCH MEMORANDUM

INVESTIGATION OF A HALF-CONICAL SCOOP INLET MOUNTED AT FIVE ALTERNATE CIRCUMFERENTIAL LOCATIONS AROUND A CIRCULAR FUSELAGE

PRESSURE-RECOVERY RESULTS AT A MACH NUMBER OF 2.01

By Lowell E. Hasel, John L. Lankford,
and A. W. Robins

Langley Aeronautical Laboratory
Langley Field, Va.

NATIONAL ADVISORY COMMITTEE FOR AERONAUTICS

WASHINGTON

June 30, 1953

[redacted]

NATIONAL ADVISORY COMMITTEE FOR AERONAUTICS

RESEARCH MEMORANDUM

INVESTIGATION OF A HALF-CONICAL SCOOP INLET MOUNTED AT FIVE ALTERNATE CIRCUMFERENTIAL LOCATIONS AROUND A CIRCULAR FUSELAGE

PRESSURE-RECOVERY RESULTS AT A MACH NUMBER OF 2.01

By Lowell E. Hasel, John L. Lankford,
and A. W. Robins

SUMMARY

The effects of inlet circumferential position around the fuselage on the characteristics of a half-conical scoop inlet having a 24.6° half-angle cone have been investigated in the Langley 4- by 4-foot supersonic pressure tunnel. Pressure-recovery results have been obtained at a Mach number of 2.01 for a fixed boundary-layer-bleed height which was 60 percent of the boundary-layer thickness at an angle of attack of 0°, and for cowling position parameters of 42.4° and 38.0°. The inlet had a capture area equal to 24.9 percent of the basic-fuselage frontal area. The angle of attack was varied from 0° to 12°.

The most favorable pressure-recovery characteristics at angles of attack were obtained with the inlet located on the bottom of the fuselage where the maximum recovery increased from a value of 81 percent at an angle of attack of 0° to 87 percent at 12°. In general, the pressure recovery decreased with increasing angle of attack for all other inlet locations. At a given angle of attack the pressure recovery decreased as the inlet location was progressively moved from the bottom to the top of the fuselage.

Stable subcritical operation of the inlet with nearly constant pressure recovery was obtained for inlet mass-flow ratios from 1.0 to about 0.76 at an angle of attack of 0° with the central body in the design position.

[redacted]

INTRODUCTION

Past research has shown that single-shock conical nose inlets with 25° or 30° half-angle cones have relatively high pressure recoveries at moderate supersonic speeds. It might be expected, therefore, that half-conical scoop inlets would also have relatively high pressure recoveries at corresponding Mach numbers. This supposition has been shown to be true (refs. 1 and 2) if most of the initial boundary layer ahead of the scoop inlet is removed. A great deal of the research on conical inlet scoops has been performed either on a flat plate at an angle of attack of 0° or with the inlet in a single position on a specific fuselage. Some evaluations have been made (ref. 3 and unpublished data) of the effect of inlet position around the fuselage circumference on performance characteristics. These data indicate that at angles of attack the circumferential location can significantly affect the inlet pressure recoveries and drag because of the varying boundary-layer thickness and local Mach number.

A more detailed investigation has therefore been undertaken in the Langley 4- by 4-foot supersonic pressure tunnel to evaluate through an angle-of-attack range the effect of inlet circumferential position on the pressure-recovery and force characteristics of a half-conical scoop inlet. The pressure-recovery results of the first phase of this investigation are presented in this report. Data have been obtained at a free-stream Mach number of 2.01 for two central-body positions, from a half-conical scoop inlet having a fixed boundary-layer bleed height equal to 0.6 of the boundary-layer thickness at an angle of attack of 0°. The inlet was located around the fuselage at five positions, equally spaced from top to bottom, and the angle of attack was varied from 0° to 12°.

SYMBOLS

A_D cross-sectional area of diffuser

A_{min} minimum cross-sectional area of diffuser (2.70 sq in. for $\theta_L = 42.4^\circ$ and 2.56 sq in. for $\theta_L = 38^\circ$)

H/H_o mass-flow-weighted total-pressure recovery

H_o free-stream total pressure

m/m_o ratio of actual mass flow through inlet to mass flow of air at free-stream conditions through a stream tube having an area equal to inlet capture area

$(m/m_o)_b$ ratio of actual mass flow through boundary-layer bleed to mass flow of air at free-stream conditions through a stream tube having an area equal to capture area of boundary-layer bleed

M local Mach number

M_o free-stream Mach number

α angle of attack, deg

ϕ circumferential location of inlet (fig. 7), deg

θ_L cowling position parameter (angle between axis of central body and line extending from tip of central body to lip of inlet), deg

MODELS

The basic fuselage, which was sting-mounted in the tunnel (fig. 1), consisted of an ogival nose section having a fineness ratio of 3.5 and a cylindrical aft section with a diameter of 4.50 inches. The over-all fineness ratio of the fuselage was 9.5.

The inlet (figs. 1 to 4) was designed with a capture area equal to 24.9 percent of the basic-fuselage frontal area. The lip of the inlet was located at fuselage station 18.00, which is 0.5 fuselage diameter behind the end of the nose section. The external and internal lip angles were 10° and 7°, respectively. A 24.6° half-angle cone formed the forward portion of the movable central body. Diffusion was obtained aft of the central body by inclining the floor of the duct toward the center of the fuselage (fig. 1), gradually changing the diffuser from a crescent to a circular shape. Figure 5 shows the area variation along the diffuser for the two positions of the central body at which tests were made. The inlet had internal contraction ratios of 10 and 0 percent for the two positions of the central body, $\theta_L = 42.4^\circ$ and 38.0°, respectively, at which tests were made. The corresponding over-all expansion ratios of the diffusers in terms of the minimum areas were 2.92 and 3.08. Mass-flow variation at each central-body position was obtained by use of a movable exit plug which was supported from the sting (fig. 6).

A rake of static- and total-pressure tubes was located in the circular constant-area section of the diffuser where the local Mach number was about 0.2 to determine the inlet mass flow and pressure-recovery characteristics.

The boundary-layer bleed height normal to the fuselage surface was 0.125 inch (figs. 2 and 4). This resulted in a bleed frontal area which was about 9 percent of the inlet capture area. The leading edge of the bleed was swept back as shown in figures 1 and 4. In a plane normal to the bleed leading edge the lip angle was about 9°. The air entering the boundary-layer bleed was turned abruptly (fig. 1) toward the fuselage center and was ducted to the model base where it was discharged from two circular ducts (fig. 6). Sting-mounted rakes were used at the exit of each duct to measure the pressure recovery and mass flow through the boundary-layer bleed. A butterfly valve was installed in the duct system to control the mass flow.

A two-tube traversing rake was installed on the fuselage to measure the boundary-layer thickness at the station corresponding to the tip of the boundary-layer bleed. The rake consisted of one static- and one total-pressure tube. These tubes were mounted 0.75 inch apart in a plane perpendicular to the fuselage surface. A static orifice was also installed in the fuselage at the same station.

TESTS AND METHODS

Tests

The tests were conducted at a Mach number of 2.01 with a stagnation pressure of 14 lb/sq in. and a stagnation temperature of 120° F. The Reynolds number based on inlet lip radius was 0.4×10^6. Moisture content of the tunnel air was kept at a value which prevented condensation effects in the test section.

Pressure-recovery and mass-flow data of the main inlet and boundary-layer bleed were obtained with the inlet located in five circumferential positions around the fuselage (fig. 7). These inlet locations were spaced at 45° intervals from the top ($\phi = 0^\circ$) to the bottom ($\phi = 180^\circ$) of the fuselage. At each inlet location, tests were conducted with the central body located at $\theta_L = 42.4^\circ$ (the design position at $\alpha = 0^\circ$) and at $\theta_L = 38.0^\circ$ (a position which limited the maximum mass flow m/m_o at $\alpha = 0^\circ$ to about 0.9). Since the Mach number across the inlet varied, the position of the conical shock changed with respect to the inlet lip at each point along the lip. At $\theta_L = 42.4^\circ$ the conical shock was very near that portion of the inlet lip which is in plane of symmetry of the inlet. In general, all data were obtained with maximum mass flow through the boundary-layer bleed and only a limited amount of data were obtained with reduced bleed mass flow. The angle of attack was varied from 0° to 12° in 3° increments.

The boundary-layer thickness at station 16.4 on the fuselage without inlet was determined at angles of attack of 0°, 6°, and 12° for all values of ϕ.

The pressure data were photographically recorded on a multiple-tube mercury manometer board. The beginning of buzz was visually determined by observing the schlieren image of the flow at the inlet.

All tests were conducted with a 0.020-inch-diameter wire located around the fuselage 0.5 inch aft of the tip of the nose. The wire served as a boundary-layer transition trip.

Reduction of Data

The pressure-recovery data were computed by a mass-flow weighting technique and are referenced to the free-stream stagnation pressure. Inlet mass-flow ratios are based on the amount of air at free-stream conditions which passes through a stream tube whose area is equal to the inlet capture area at $\alpha = 0^{\circ}$. Mass-flow ratios of the boundary-layer bleed are similarly based on the capture area of the boundary-layer bleed.

The outer edge of the boundary layer (figs. 8 and 9) was assumed to be at the point where the velocity of the boundary-layer air was 99 percent of the local stream velocity. For the data presented in figure 10 the local Mach numbers at the outer edge of the boundary layer were calculated on the assumption that the static pressures measured on the fuselage were constant across the boundary layer. For the data presented in figure 11 the Mach numbers were determined both from the fuselage static pressure and the rake static pressures.

Accuracy

The accuracy of the data is estimated to be as follows:

α, deg	±0.10
H/H_o	±0.02
m/m_o	±0.04

RESULTS AND DISCUSSION

Flow Surveys on Fuselage

Flow surveys were made at fuselage station 16.4 without the inlet installed to determine the boundary-layer thickness and local Mach numbers at the inlet. This station corresponds to the tip of the boundary-layer bleed. The results of these surveys are presented in figures 8 to 11. Figures 8 to 10 show the effect of angle of attack and inlet position on the boundary-layer thickness and the local Mach number at the outer edge of the boundary layer. Figure 11 presents the radial variation of the local Mach number and local total-pressure ratio across the entire inlet at $\alpha = 0^{\circ}$.

The data presented in figures 8 to 10 show that both the boundary-layer thickness and the local Mach number ahead of the inlet vary appreciably with circumferential location and angle of attack. At $\phi = 135^{\circ}$ and 180° the boundary-layer thickness becomes less than the boundary-layer-bleed height for angles of attack greater than about 4°. The local Mach number also appears lowest at these two circumferential positions. At $\phi = 0^{\circ}$ the boundary-layer thickness increases rapidly as α increases and at 12° is about 50 percent of the inlet lip radius. These data indicate that, from the standpoint of obtaining maximum pressure recovery at angles of attack, the bottom of the fuselage ($\phi = 180^{\circ}$) appears to be the most favorable inlet location because of the relatively thin boundary layer and lower local Mach number. At the higher angles of attack (fig. 9) the boundary layer thickens rapidly at values of ϕ less than about 60°. It would appear, therefore, that from boundary-layer considerations alone the inlet should have satisfactory pressure-recovery characteristics for values of ϕ between 180° and about 60°. It should be mentioned that at angles of attack these data represent the flow characteristics only along a radial line passing through the tip of the boundary-layer bleed and not across the entire inlet width.

The complete flow survey (fig. 11) indicates that at $\alpha = 0^{\circ}$ the Mach number ahead of the inlet varies from 2.08 to 2.02 (exclusive of the boundary layer).

Pressure-Recovery Characteristics

The pressure-recovery data which were obtained with the central body in the design position, $\theta_L = 42.4^{\circ}$, are presented in figure 12. The corresponding data obtained with the central body forward, $\theta_L = 38^{\circ}$, so that the maximum value of m/m_o was about 0.9 are presented in figure 13.

Stable range of operation is indicated by the solid lines in these figures. The dashed portions of these curves indicate instability or buzz. No data for stable operation were obtained at the conditions for which one or two points are indicated with dashes on either side. There is a possibility that some stable range of operation would have been found in these cases at higher values of m/m_o.

These data were obtained with the boundary-layer bleed operating at its maximum capacity. It should be mentioned, however, that at maximum capacity the boundary-layer removal system may not have been removing all of the air passing through an area equal to the boundary-layer-bleed capture area. At $\alpha = 0^\circ$, for example, about 85 percent of this air was removed. The remainder was either swept aside by the bleed or entered the inlet.

The inlet pressure-recovery and mass-flow data presented in figures 12 and 13, and the corresponding boundary-layer mass-flow ratios, are given in table I.

<u>Maximum pressure recovery</u>.- An index of the effect of circumferential position on maximum pressure recovery with the central body in the design position is given by figure 14. Only stable operating conditions are shown. The maximum pressure recovery at $\alpha = 0^\circ$ is about 81 percent. This maximum recovery is lower than data obtained from similar inlets tested on flat plates at a slightly lower Mach number (refs. 1 and 2). Some of this decrease in pressure recovery is probably due to the inadequate boundary-layer bleed height which did not permit the removal of the outermost portion of the boundary layer (see fig. 8). Furthermore, the lip angle of the top of the boundary-layer bleed (fig. 2) is too large to permit an attached shock to exist. A normal shock must therefore be decreasing the pressure recovery of the air entering near the floor of the inlet. The sharp corner which exists at the intersection of the inlet cowling and inlet floor may also be causing additional pressure losses (ref. 4). The curves of figure 14 indicate that the pressure recovery decreases at the $\phi = 0^\circ$, $\phi = 45^\circ$, and $\phi = 90^\circ$ positions as the angle of attack increases. In the $\phi = 135^\circ$ position the pressure recovery increases slightly and then decreases as the angle of attack increases. At $\phi = 180^\circ$ (the best position from pressure-recovery considerations) the maximum recovery (fig. 12(e)) increases with α and reaches a value of 87 percent at $\alpha = 12^\circ$. At a given angle of attack the pressure recovery decreases as the inlet position is progressively moved from $\phi = 180^\circ$ toward $\phi = 0^\circ$.

It has previously been mentioned (fig. 9) that at angles of attack the adverse effects of the boundary layer on the inlet pressure recovery should not be large if the inlet is located at values of ϕ greater than about 60°. The data presented in figure 14, however, show relatively large decreases in pressure recovery at $\phi = 90^\circ$, indicating that other effects such as high local Mach number and large cross-flow angles can also adversely affect the inlet pressure recovery. At the $\phi = 0^\circ$ and $\phi = 45^\circ$ positions the thick boundary layer (fig. 9) apparently reduced the pressure recovery and induced instability. Greater boundary-layer bleed heights might alleviate this condition. At $\phi = 0^{\circ}$, increasing the fineness ratio of the fuselage ahead of the inlet might improve the pressure recoveries at the higher angles of attack. Unpublished data which have been obtained from scoop inlets having body fineness ratios ahead of the inlet of 5 or larger have indicated that at angles of attack of about 9° or more the formation of vortices due to viscous cross-flow effects may improve the inlet pressure recoveries ($\phi = 0^{\circ}$) by thinning the boundary layer in this region.

An interesting aspect indicated by figure 14 is the existence of a circumferential position (approx. $\phi = 160^{\circ}$) that would give nearly constant values of pressure recovery for angles of attack through 9°.

Although the data presented in figure 14 indicate an optimum position from pressure-recovery considerations, it must be remembered that the final evaluation of the best inlet location should be made on a thrust-minus-drag basis.

The maximum pressure-recovery values for the central body in the off-design condition ($\theta_L = 38^{\circ}$ and theoretical maximum value of $m/m_o \approx 0.9$ at $\alpha = 0^{\circ}$) are cross-plotted in figure 15. The values for $\phi = 0^{\circ}$, $\phi = 45^{\circ}$, and $\phi = 90^{\circ}$ show no large differences from those for the design condition. The values at angles of attack for $\phi = 135^{\circ}$ and $\phi = 180^{\circ}$ are lower than the recoveries for design conditions.

<u>Local pressure recovery</u>.- Representative local pressure-recovery contours in the subsonic diffuser are presented in figure 16. These data, which were obtained with the central body in the design position, indicate that for certain conditions separated flow exists in the diffuser. Furthermore, the lack of flow symmetry is apparent in most of the contours. The distribution appears to be most uniform at $\phi = 180^{\circ}$.

<u>The effect of boundary-layer-bleed mass-flow variation</u>.- The effect of varying the boundary-layer-bleed mass flow is shown in figure 17. These data indicate that for this model configuration and at these angles of attack little additional pressure recovery could have been gained by removing more of the boundary-layer air. The dashed line indicates the value of the boundary-layer-bleed mass-flow ratio $(m/m_o)_b$ at which all of the boundary air in the capture area of the bleed would have been removed at $\alpha = 0^{\circ}$.

<u>Inlet buzz</u>.- Stable subcritical operation of the inlet with nearly constant pressure recovery was obtained at $\alpha = 0^{\circ}$ (fig. 12) with the central body in the design position ($\theta_L = 42.4^{\circ}$) for values of m/m_o from 1.0 to about 0.76. It appears that the vortex sheet which forms

downstream of the intersection of the normal shock and conical shock entered the inlet without affecting the inlet stability. This vortex sheet normally triggers buzz, if at all, as soon as it enters the inlet (ref. 5). On the present configuration, however, the 10-percent internal contraction (fig. 5) may have assisted in preventing this type of buzz because of the requirement that several percent of mass flow be spilled as soon as the inlet becomes subcritical. The resultant forward movement of the normal shock may have moved the vortex sheet far enough away from the diffuser surface to prevent buzz. Stable subcritical ranges of operation have also been observed for a half-conical scoop inlet in reference 1 and for conical-nose inlets in references 6 and 7. The latter inlets had either very little or no internal contraction. Reference 6 indicates that the rate of expansion of the initial portion of the diffuser aft of the minimum section may influence the stability range. A similar range of stable operation was not observed at angles of attack, but some subcritical regulation is possible at low angles of attack (fig. 12).

The stability at higher angles of attack generally increased with increasing values of ϕ except for $\phi = 135^\circ$, for the design position of the central body.

The stability range for the off-design condition ($\theta_L = 38^\circ$) at $\alpha = 0^\circ$ is considerably less than the range at design condition. In some cases at angle of attack, however (e.g., figs. 12(b) and 13(b) at 9° and figs. 12(d) and 13(d) at 12°) stable subcritical mass-flow regulation was found with the central body in the off-design position but was not observed with the central body in the design position. For the latter configuration, stable operation might have been obtained in some cases at higher mass-flow ratios.

At $\phi = 90^\circ$, where cross flow is present, an interesting stability pattern was observed. As the angle was increased from $\alpha = 0^\circ$ to $\alpha = 12^\circ$ the stability range was at first reduced and then began to increase at the higher angles. (See figs. 12(c) and 13(c).) This trend is also evident to a lesser extent at other values of ϕ.

The stability at higher angles of attack increased with increasing values of ϕ for the off-design condition.

CONCLUDING REMARKS

The effects of inlet circumferential position around the fuselage on the pressure-recovery characteristics of a half-conical scoop inlet have been investigated at a Mach number of 2.01. Data were obtained from a half-conical scoop inlet having a fixed boundary-layer bleed height which was 60 percent of the boundary-layer thickness at an angle of attack of 0°. The angle of attack was varied from 0° to 12°.

The data indicate that:

1. The most favorable pressure-recovery characteristics were obtained with the inlet located on the bottom of the fuselage where the maximum recovery increased from a value of 81 percent at an angle of attack of 0° to a value of 87 percent at 12°. In general, a decrease in pressure recovery with angle of attack was observed for all other inlet locations.

2. At a given angle of attack the pressure recovery decreases as the inlet location was progressively moved from the bottom to the top of the fuselage.

3. Stable subcritical operation of the inlet with nearly constant pressure recovery was obtained for inlet mass-flow ratios from 1.0 to about 0.76 at an angle of attack of 0° with the central body in the design position.

Langley Aeronautical Laboratory,
National Advisory Committee for Aeronautics,
Langley Field, Va.

REFERENCES

1. Wittliff, Charles E., and Byrne, Robert W.: Preliminary Investigation of a Supersonic Scoop Inlet Derived From a Conical-Spike Nose Inlet. NACA RM L51G11, 1951.

2. Goelzer, H. Fred, and Cortright, Edgar M., Jr.: Investigation at Mach Number 1.88 of Half of a Conical-Spike Diffuser Mounted As a Side Inlet With Boundary-Layer Control. NACA RM E51G06, 1951.

3. Schaefer, Raymond F.: Some Design Considerations for Half-Round Side Inlets. Wright Aero. Rep. No. 1692, Supersonic Inlet Symposium, Curtiss-Wright Corp. (Wood-Ridge, N. J.), Jan. 23, 1953.

4. Valerino, Alfred S.: Effects of Internal Corner Fillets on Pressure Recovery - Mass Flow Characteristics of Scoop-Type Conical Supersonic Inlets. NACA RM E52J10, 1952.

5. Ferri, Antonio, and Nucci, Louis M.: The Origin of Aerodynamic Instability of Supersonic Inlets at Subcritical Conditions. NACA RM L50K30, 1951.

6. Weinstein, Maynard I., and Davids, Joseph: Force and Pressure Characteristics for a Series of Nose Inlets at Mach Numbers From 1.59 to 1.99. III - Conical-Spike All-External-Compression Inlet With Supersonic Cowl Lip. NACA RM E50J30, 1951.

7. Beke, Andrew, and Allen, J. L.: Force and Pressure-Recovery Characteristics of a Conical-Type Nose Inlet Operating at Mach Numbers of 1.6 to 2.0 and at Angles of Attack to 9°. NACA RM E52I30, 1952.

TABLE I.- INLET MASS-FLOW AND PRESSURE-RECOVERY DATA

PRESENTED IN FIGURES 12 AND 13 AND CORRESPONDING

BOUNDARY-LAYER-BLEED MASS-FLOW DATA

θ_L, deg	ϕ, deg	α, deg	m/m_o	H/H_o	$(m/m_o)_b$
42.4	0	0	1.008	0.810	0.521
42.4	0	0	.996	.808	.518
42.4	0	0	.944	.813	.535
42.4	0	0	.890	.806	.541
42.4	0	0	.870	.811	.536
42.4	0	0	.786	.805	.535
42.4	0	0	.763	.807	.504
42.4	0	0	.713	.704	.425
42.4	0	3	1.036	.749	.521
42.4	0	3	1.006	.751	.504
42.4	0	3	.957	.733	.482
42.4	0	6	.967	.626	.366
42.4	0	12	.869	.516	.308
42.4	45	3	1.080	.755	.485
42.4	45	3	1.061	.762	.485
42.4	45	3	1.049	.764	.489
42.4	45	3	1.018	.769	.487
42.4	45	6	1.098	.722	.474
42.4	45	6	1.098	.717	.456
42.4	45	6	1.080	.713	.463
42.4	45	9	1.004	.623	.377
42.4	45	12	.892	.486	.309
42.4	90	3	1.047	.784	.498
42.4	90	3	1.034	.780	.534
42.4	90	3	.984	.793	.549
42.4	90	3	.902	.765	.534
42.4	90	3	.895	.788	.507
42.4	90	3	.869	.777	.501
42.4	90	3	.863	.795	.501
42.4	90	6	1.084	.723	.526
42.4	90	6	1.009	.751	.533
42.4	90	6	.962	.760	.529
42.4	90	6	.949	.765	.550
42.4	90	6	.920	.632	.587

NACA

TABLE I.- INLET MASS-FLOW AND PRESSURE-RECOVERY DATA

PRESENTED IN FIGURES 12 AND 13 AND CORRESPONDING

BOUNDARY-LAYER-BLEED MASS-FLOW DATA - Continued

θ_L, deg	ϕ, deg	α, deg	m/m_o	H/H_o	$(m/m_o)_b$
42.4	90	9	0.959	0.683	0.493
42.4	90	9	.949	.706	.550
42.4	90	9	.804	.606	.572
42.4	90	9	.791	.605	.586
42.4	90	9	.700	.592	.530
42.4	90	9	.684	.584	.563
42.4	90	9	.674	.584	.554
42.4	90	12	.845	.600	.544
42.4	90	12	.830	.588	.555
42.4	90	12	.772	.591	.548
42.4	90	12	.760	.598	.573
42.4	90	12	.710	.613	.550
42.4	90	12	.662	.614	.535
42.4	90	12	.640	.623	.534
42.4	135	3	1.013	.823	.521
42.4	135	3	.942	.807	.514
42.4	135	3	.938	.815	.512
42.4	135	3	.937	.794	.506
42.4	135	3	.920	.793	.542
42.4	135	6	1.020	.764	.561
42.4	135	6	.953	.797	.546
42.4	135	6	.911	.800	.537
42.4	135	6	.910	.804	.545
42.4	135	9	.956	.774	.569
42.4	135	9	.841	.783	.555
42.4	135	12	.996	.741	.578
42.4	180	3	.983	.806	.520
42.4	180	3	.974	.825	.544
42.4	180	3	.964	.832	.565
42.4	180	3	.930	.823	.624
42.4	180	6	1.052	.821	.603
42.4	180	6	1.031	.845	.622
42.4	180	6	1.019	.837	.614
42.4	180	6	1.000	.844	.590
42.4	180	6	.975	.838	.607
42.4	180	6	.967	.837	.589

NACA

TABLE I.- INLET MASS-FLOW AND PRESSURE-RECOVERY DATA PRESENTED IN FIGURES 12 AND 13 AND CORRESPONDING BOUNDARY-LAYER-BLEED MASS-FLOW DATA - Continued

θ_L, deg	ϕ, deg	α, deg	m/m_o	H/H_o	$(m/m_o)_b$
42.4	180	9	0.972	0.842	0.630
42.4	180	9	.965	.840	.694
42.4	180	12	.974	.862	.717
42.4	180	12	.946	.864	.732
42.4	180	12	.884	.854	.750
38.0	0	0	.846	.759	.536
38.0	0	0	.841	.786	.552
38.0	0	0	.770	.797	.562
38.0	0	3	.898	.709	.490
38.0	0	3	.895	.722	.500
38.0	0	3	.839	.746	.503
38.0	0	3	.807	.705	.436
38.0	0	6	.936	.661	.469
38.0	0	6	.926	.659	.441
38.0	0	9	.878	.608	.397
38.0	0	9	.854	.612	.398
38.0	0	12	.812	.510	.355
38.0	45	3	.967	.722	.482
38.0	45	3	.894	.733	.491
38.0	45	3	.884	.756	.476
38.0	45	3	.845	.772	.491
38.0	45	3	.821	.784	.484
38.0	45	6	.962	.696	.475
38.0	45	6	.918	.713	.473
38.0	45	6	.867	.731	.473
38.0	45	6	.795	.653	.396
38.0	45	9	.949	.645	.445
38.0	45	9	.939	.642	.454
38.0	45	9	.914	.654	.433
38.0	45	9	.862	.661	.432
38.0	45	12	.845	.498	.322
38.0	45	12	.801	.486	.313

TABLE I.- INLET MASS-FLOW AND PRESSURE-RECOVERY DATA

PRESENTED IN FIGURES 12 AND 13 AND CORRESPONDING

BOUNDARY-LAYER-BLEED MASS-FLOW DATA - Continued

θ_L, deg	ϕ, deg	α, deg	m/m_o	H/H_o	$(m/m_o)_b$
38.0	90	3	0.876	0.754	0.550
38.0	90	3	.812	.787	.545
38.0	90	3	.809	.791	.550
38.0	90	3	.785	.783	.553
38.0	90	6	.882	.729	.572
38.0	90	6	.874	.737	.559
38.0	90	6	.861	.743	.564
38.0	90	6	.854	.749	.581
38.0	90	6	.831	.745	.573
38.0	90	9	.839	.683	.552
38.0	90	9	.830	.681	.536
38.0	90	9	.810	.611	.553
38.0	90	9	.633	.574	.550
38.0	90	12	.838	.580	.530
38.0	90	12	.832	.581	.543
38.0	90	12	.780	.567	.561
38.0	90	12	.764	.565	.559
38.0	90	12	.740	.596	.500
38.0	90	12	.727	.565	.561
38.0	90	12	.709	.566	.551
38.0	90	12	.670	.573	.554
38.0	90	12	.644	.587	.475
38.0	90	12	.576	.603	.447
38.0	135	3	.898	.750	.575
38.0	135	3	.898	.737	.547
38.0	135	3	.866	.775	.551
38.0	135	3	.853	.782	.558
38.0	135	3	.837	.787	.534
38.0	135	6	.939	.735	.585
38.0	135	6	.918	.745	.574
38.0	135	6	.883	.767	.575
38.0	135	6	.837	.766	.573
38.0	135	9	.894	.723	.572
38.0	135	9	.872	.749	.571
38.0	135	9	.858	.732	.581
38.0	135	9	.814	.758	.584

TABLE I.- INLET MASS-FLOW AND PRESSURE-RECOVERY DATA

PRESENTED IN FIGURES 12 AND 13 AND CORRESPONDING

BOUNDARY-LAYER-BLEED MASS-FLOW DATA - Concluded

θ_L, deg	ϕ, deg	α, deg	m/m_o	H/H_o	$(m/m_o)_b$
38.0	135	12	0.903	0.717	0.591
38.0	135	12	.821	.733	.600
38.0	135	12	.793	.731	.605
38.0	180	3	.923	.754	.586
38.0	180	3	.896	.803	.592
38.0	180	3	.893	.739	.576
38.0	180	3	.878	.780	.600
38.0	180	3	.875	.807	.602
38.0	180	6	.955	.750	.629
38.0	180	6	.939	.764	.642
38.0	180	6	.907	.788	.635
38.0	180	6	.884	.810	.643
38.0	180	6	.852	.782	.684
38.0	180	9	.974	.760	.682
38.0	180	9	.952	.772	.683
38.0	180	9	.932	.794	.691
38.0	180	9	.902	.817	.693
38.0	180	9	.881	.781	.735
38.0	180	9	.839	.811	.702
38.0	180	12	.981	.779	.733
38.0	180	12	.945	.805	.742
38.0	180	12	.901	.820	.774
38.0	180	12	.879	.799	.785
38.0	180	12	.877	.822	.746

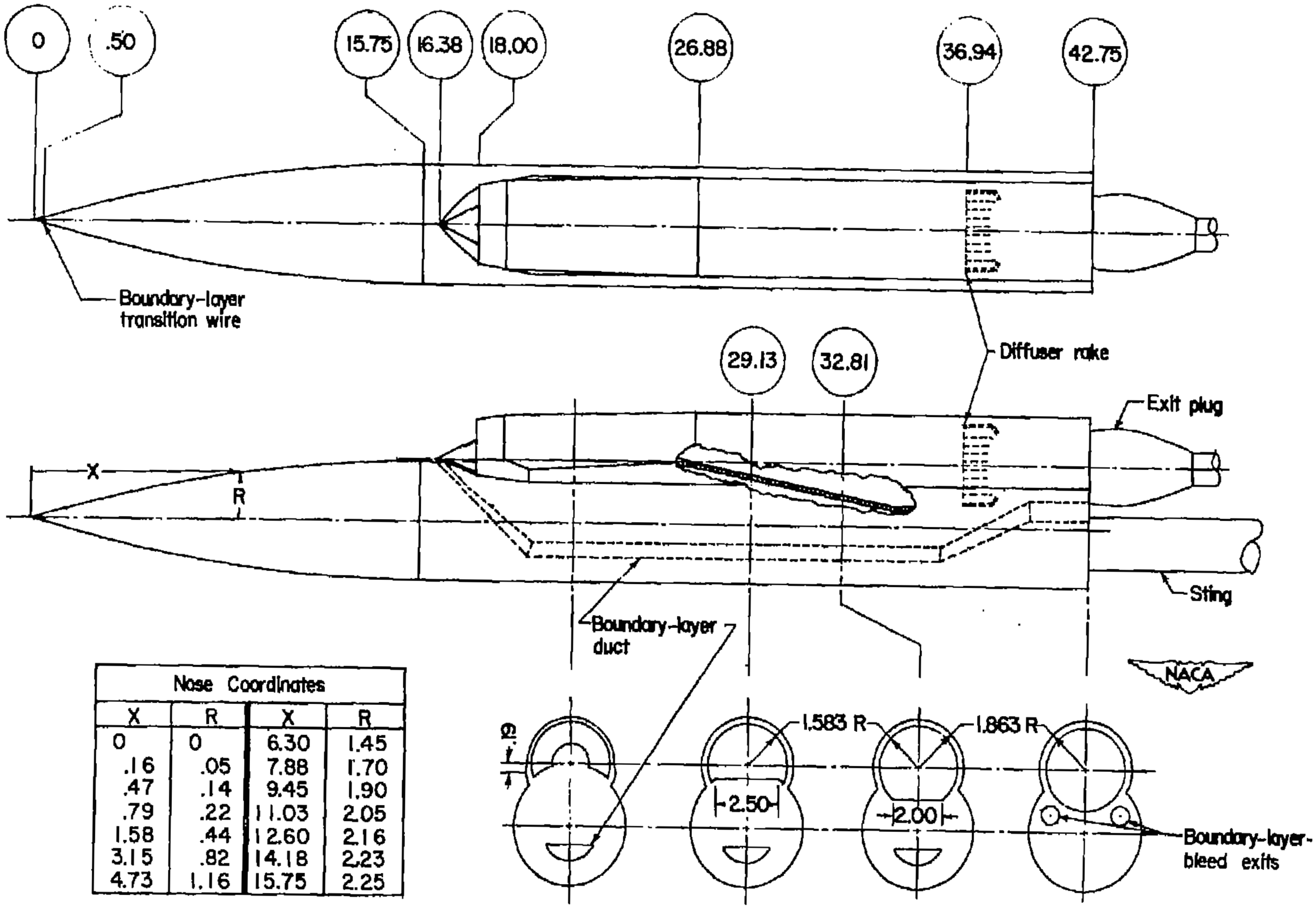

Nose Coordinates			
X	R	X	R
0	0	6.30	1.45
.16	.05	7.88	1.70
.47	.14	9.45	1.90
.79	.22	11.03	2.05
1.58	.44	12.60	2.16
3.15	.82	14.18	2.23
4.73	1.16	15.75	2.25

Figure 1.- Drawing of scoop model. All dimensions are in inches.

[redacted]

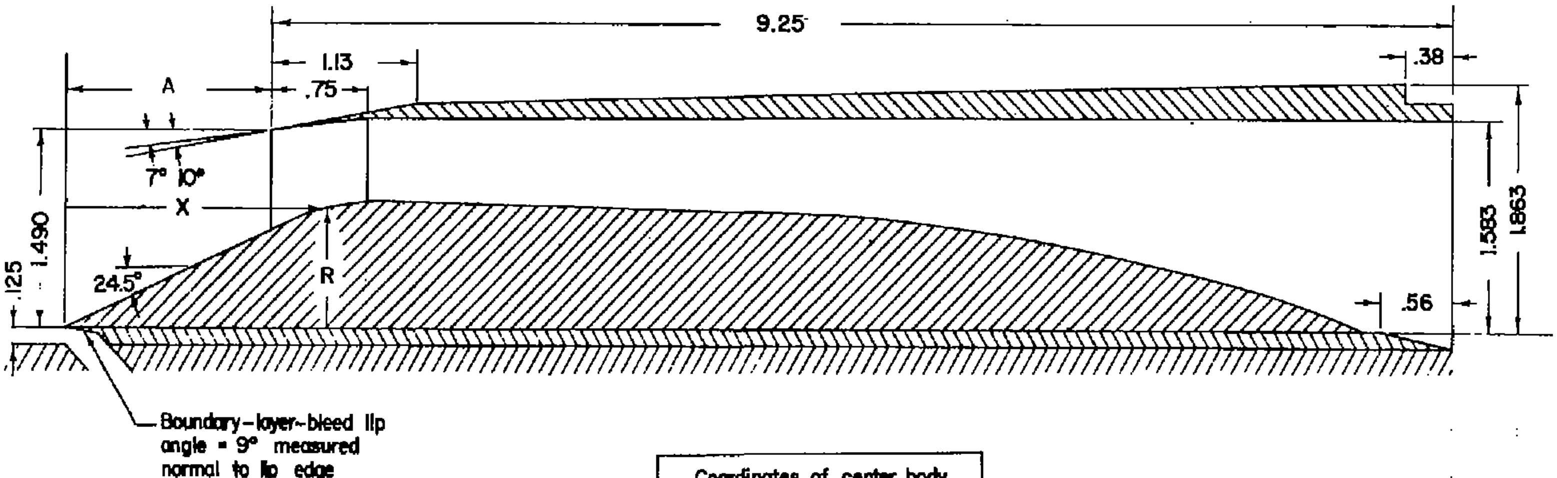

Cone position	
θ_L	A
42.4°	1.63
38.0°	1.91

Coordinates of center body			
X	R	X	R
0	0	6.92	0.77
1.86	0.85	7.42	.70
2.05	.91	7.92	.61
2.24	.94	8.42	.51
2.42	.96	8.92	.40
3.42	.94	9.42	.27
4.42	.91	9.92	.10
5.42	.88	10.17	0
6.42	.83		

Figure 2.- Details of inlet of scoop model. All dimensions are in inches.

[redacted]

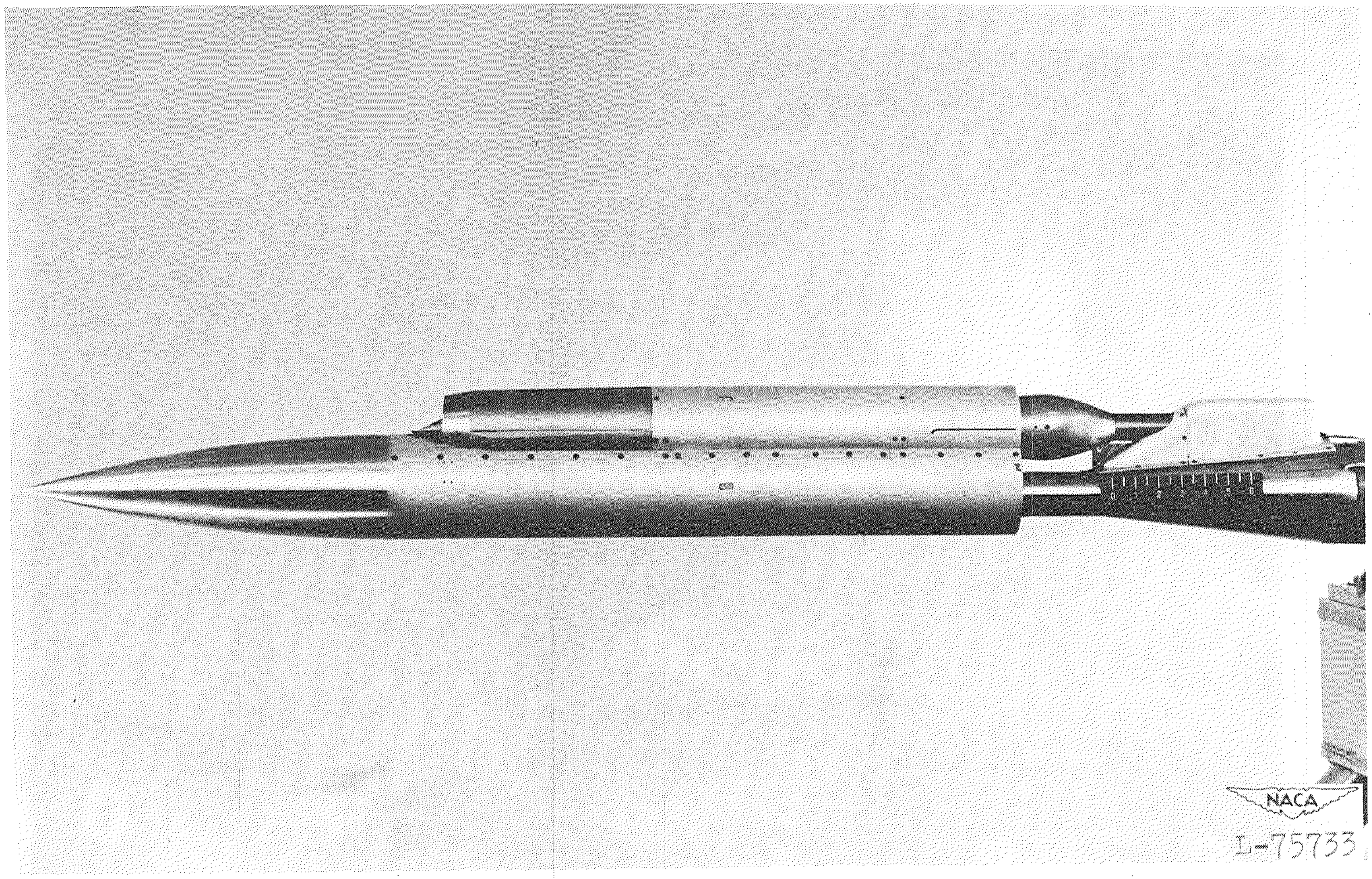

Figure 3.- Photograph of scoop model.

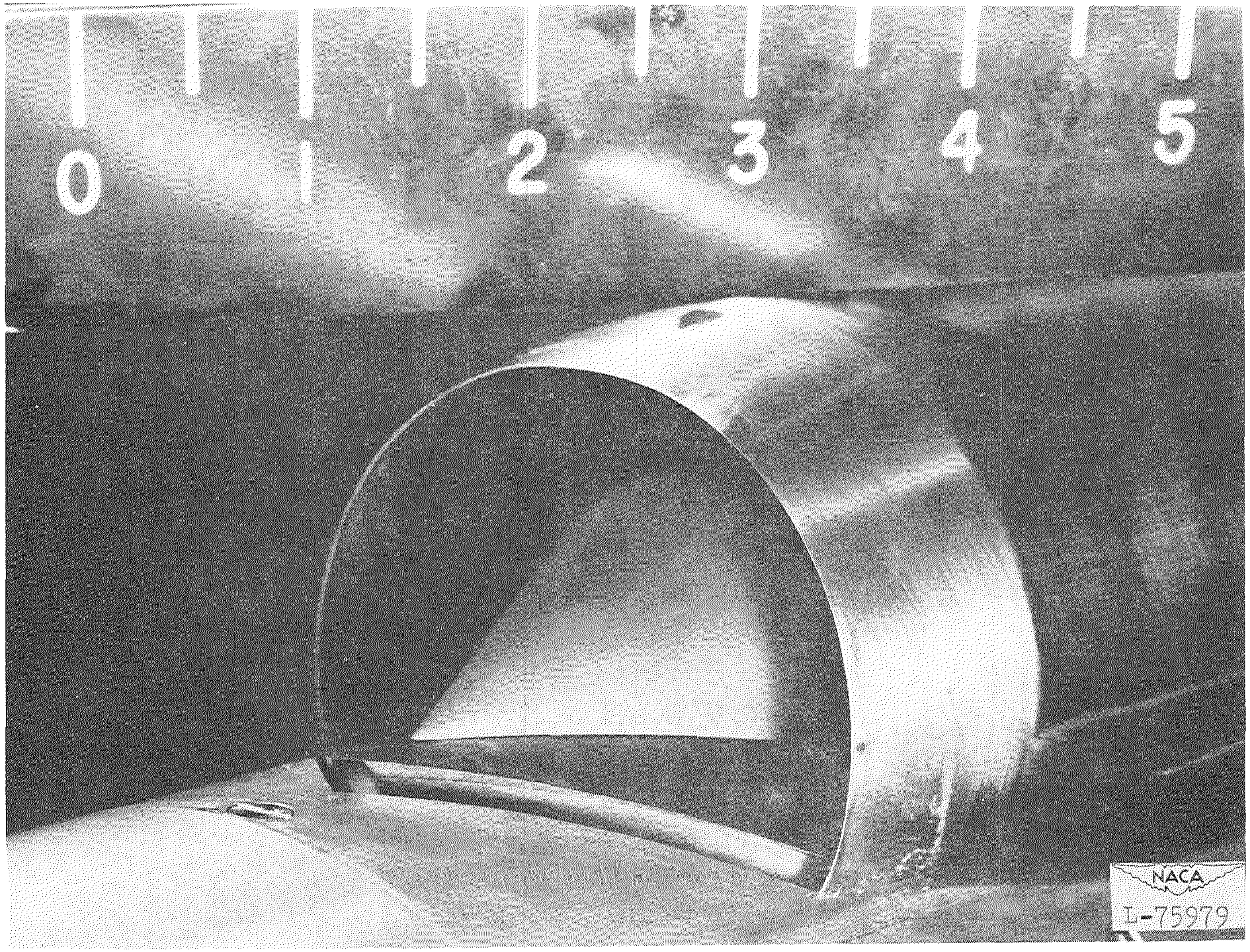

Figure 4.- Photograph of inlet of scoop model.

CONFIDENTIAL

[redacted]

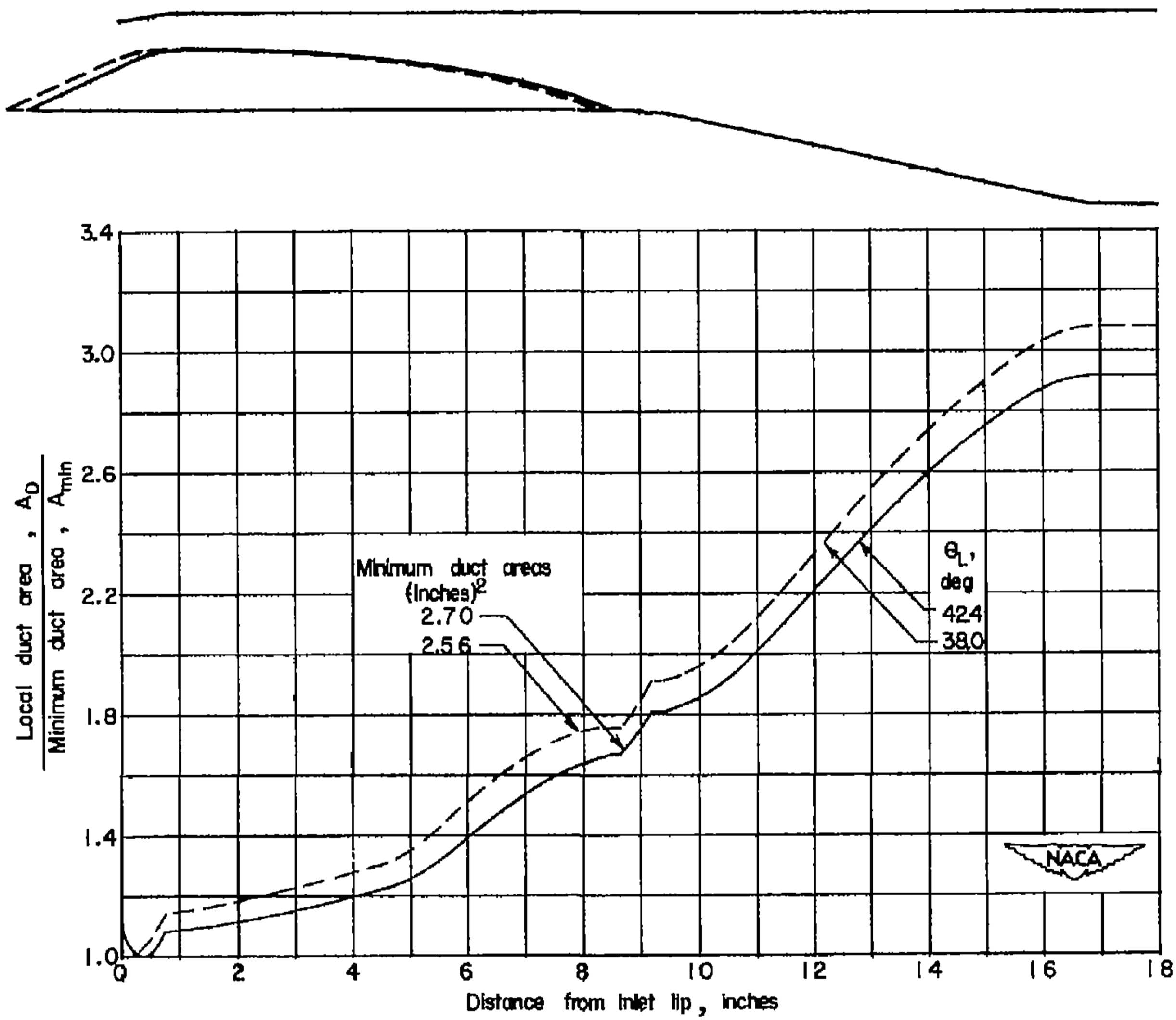

Figure 5.- Variation of A_D/A_{min} with longitudinal station for the two locations of the inlet central body.

[redacted]

CONFIDENTIAL

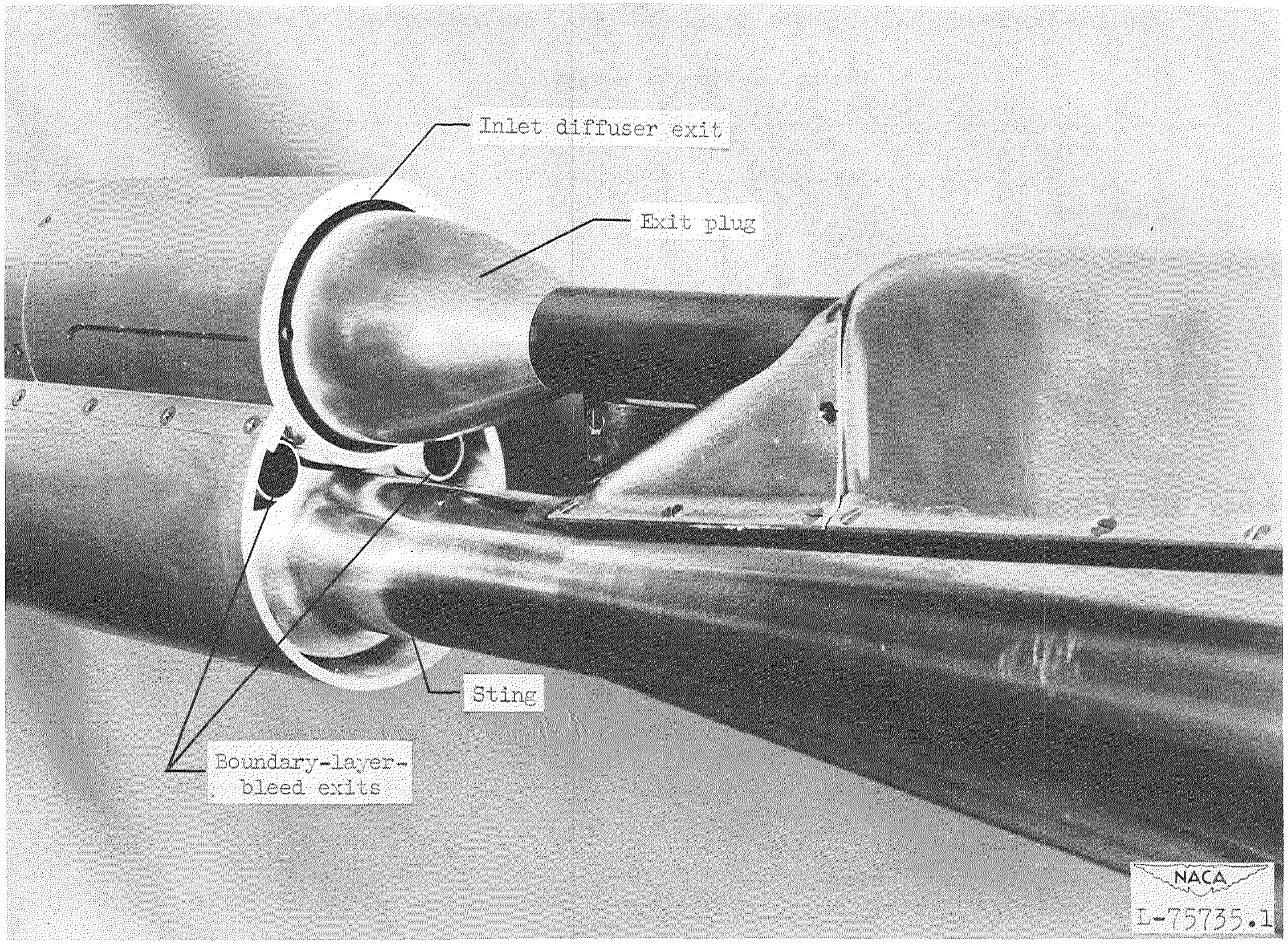

Figure 6.- Photograph of base of scoop model.

CONFIDENTIAL

[redacted]

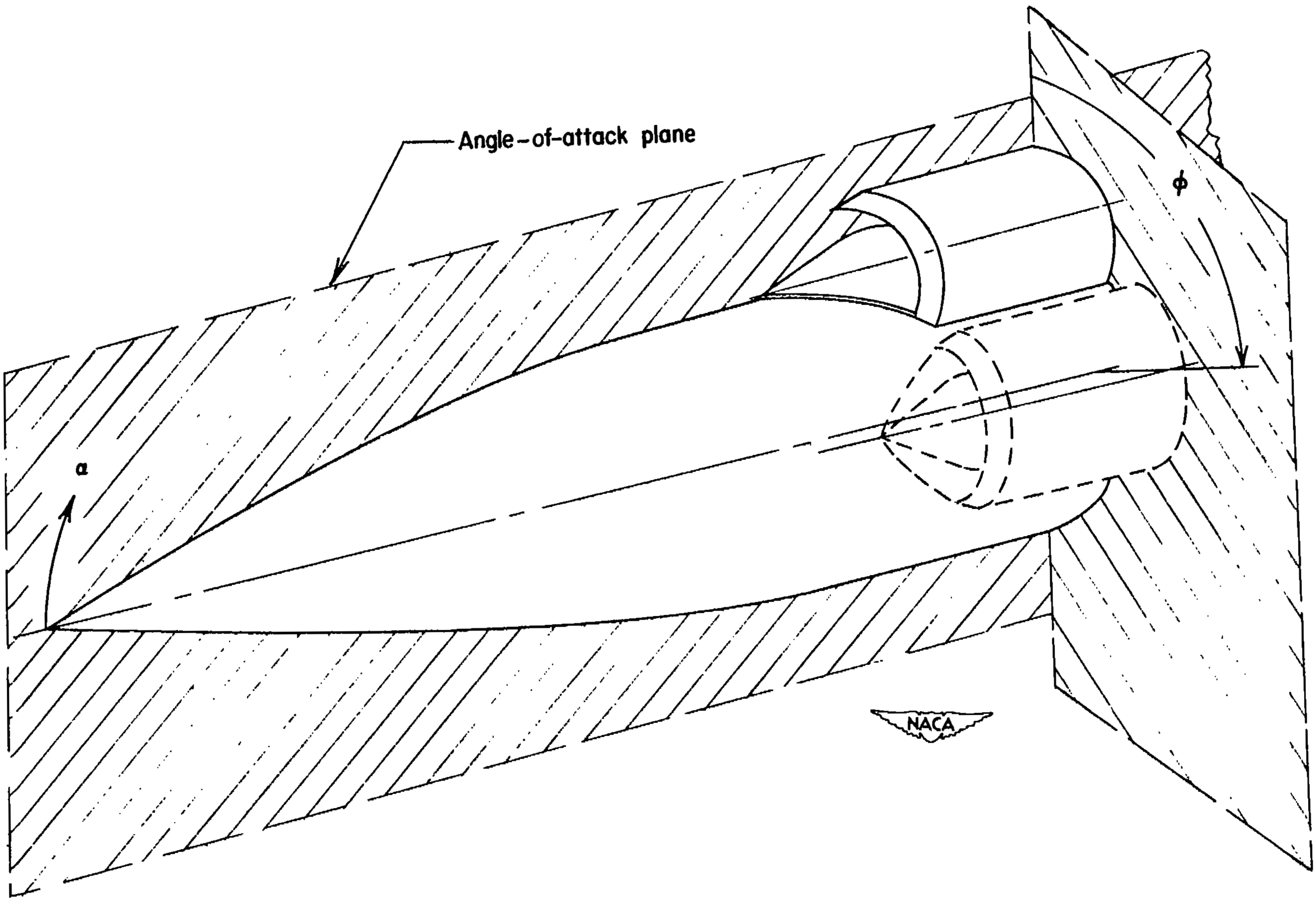

Figure 7.- Sketch showing relationship between inlet circumferential position and angle-of-attack plane.

[redacted]

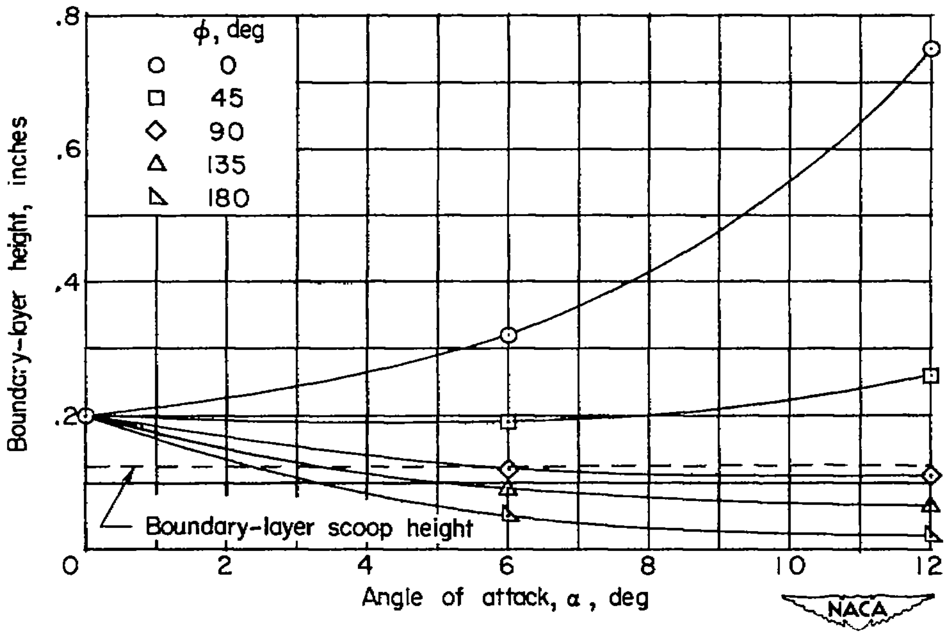

Figure 8.- Variation of boundary-layer thickness at station 16.4 on the fuselage without inlet with angle of attack and circumferential position around the fuselage.

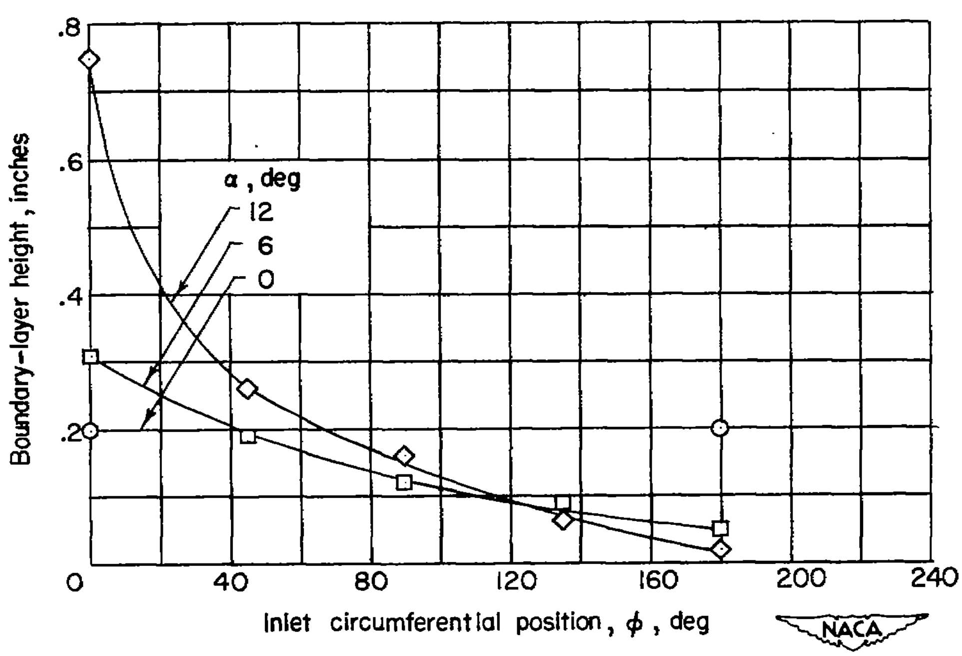

Figure 9.- Variation of boundary-layer thickness at station 16.4 on the fuselage without inlet with circumferential position around the fuselage for several angles of attack.

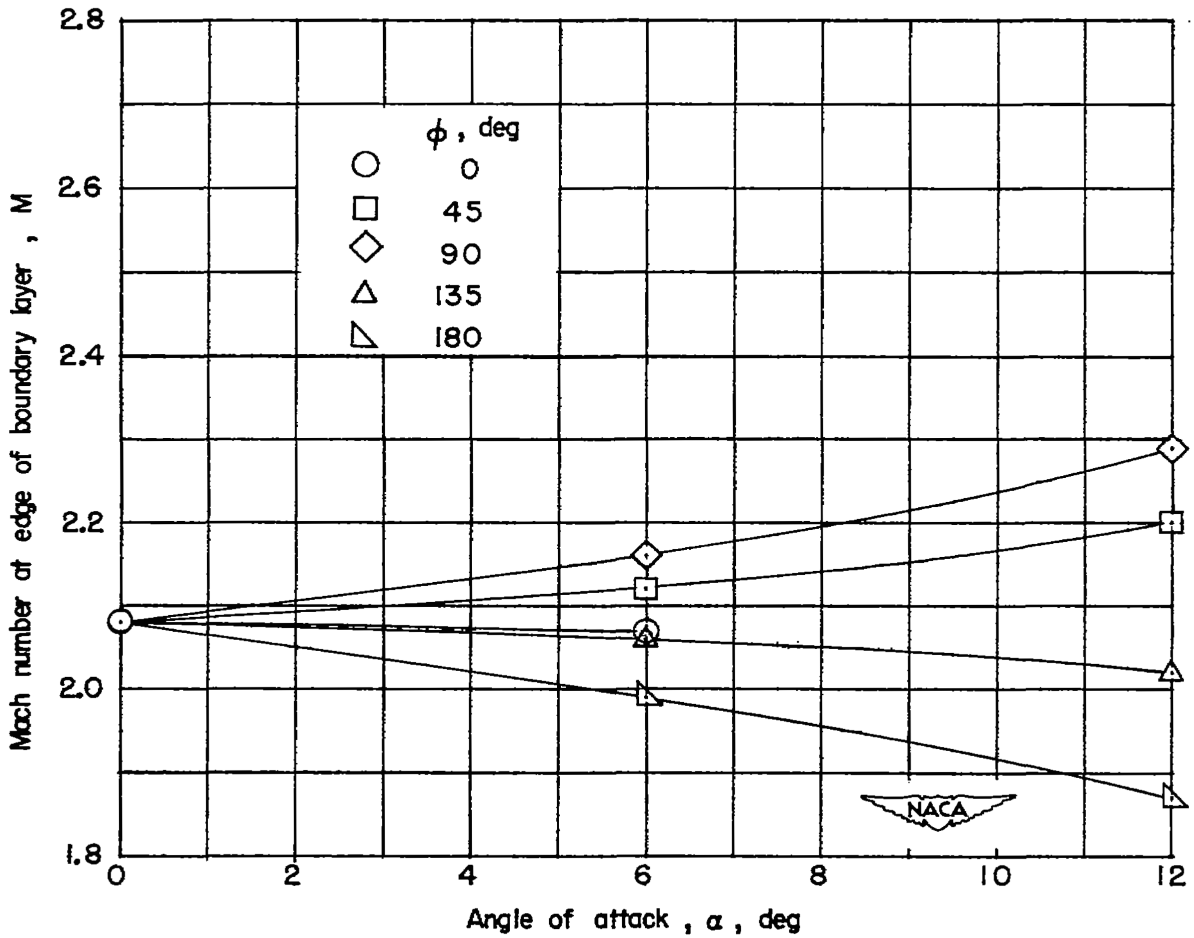

Figure 10.- Variation of local Mach number at the outer edge of the boundary layer at station 16.4 on the fuselage without inlet with angle of attack, for several circumferential positions around the fuselage.

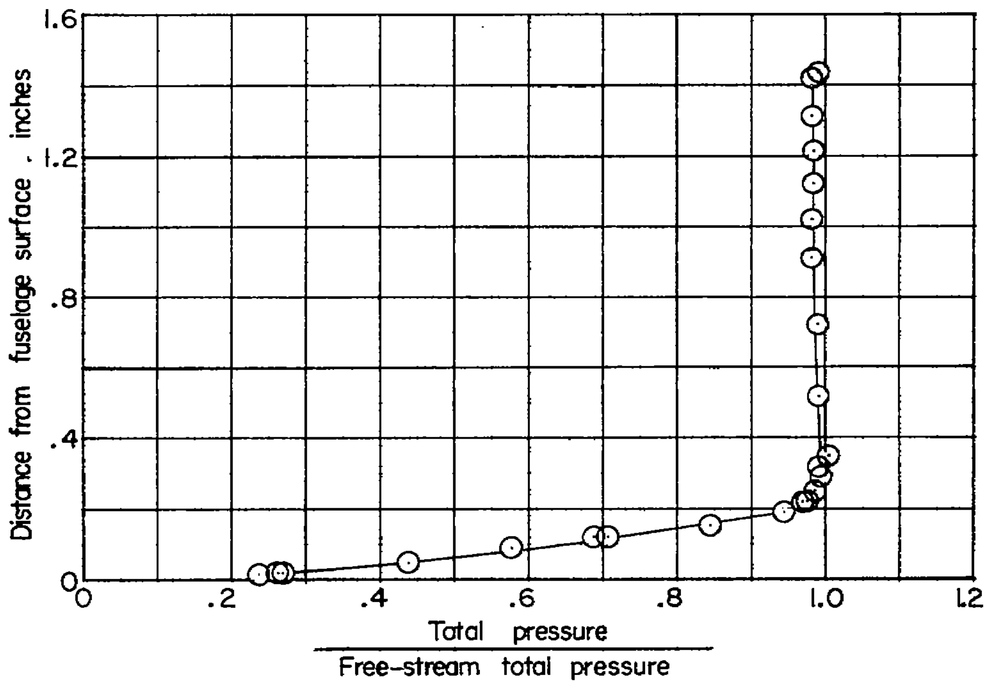

a) Local total-pressure distribution.

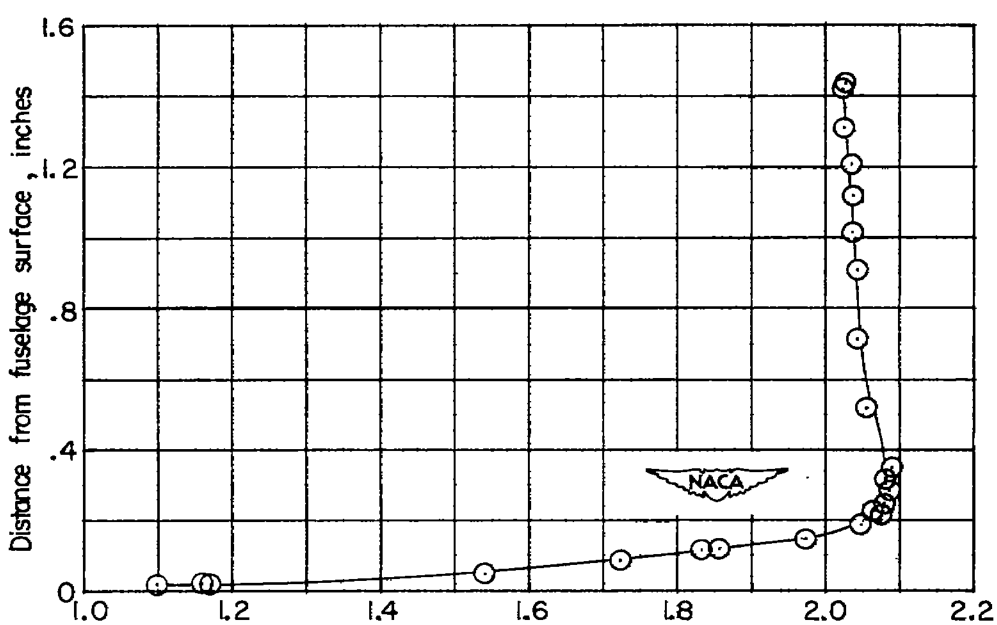

b) Local Mach number.

Figure 11.- Local flow conditions at station 16.4 on the fuselage without inlet. $\alpha = 0^{\circ}$.

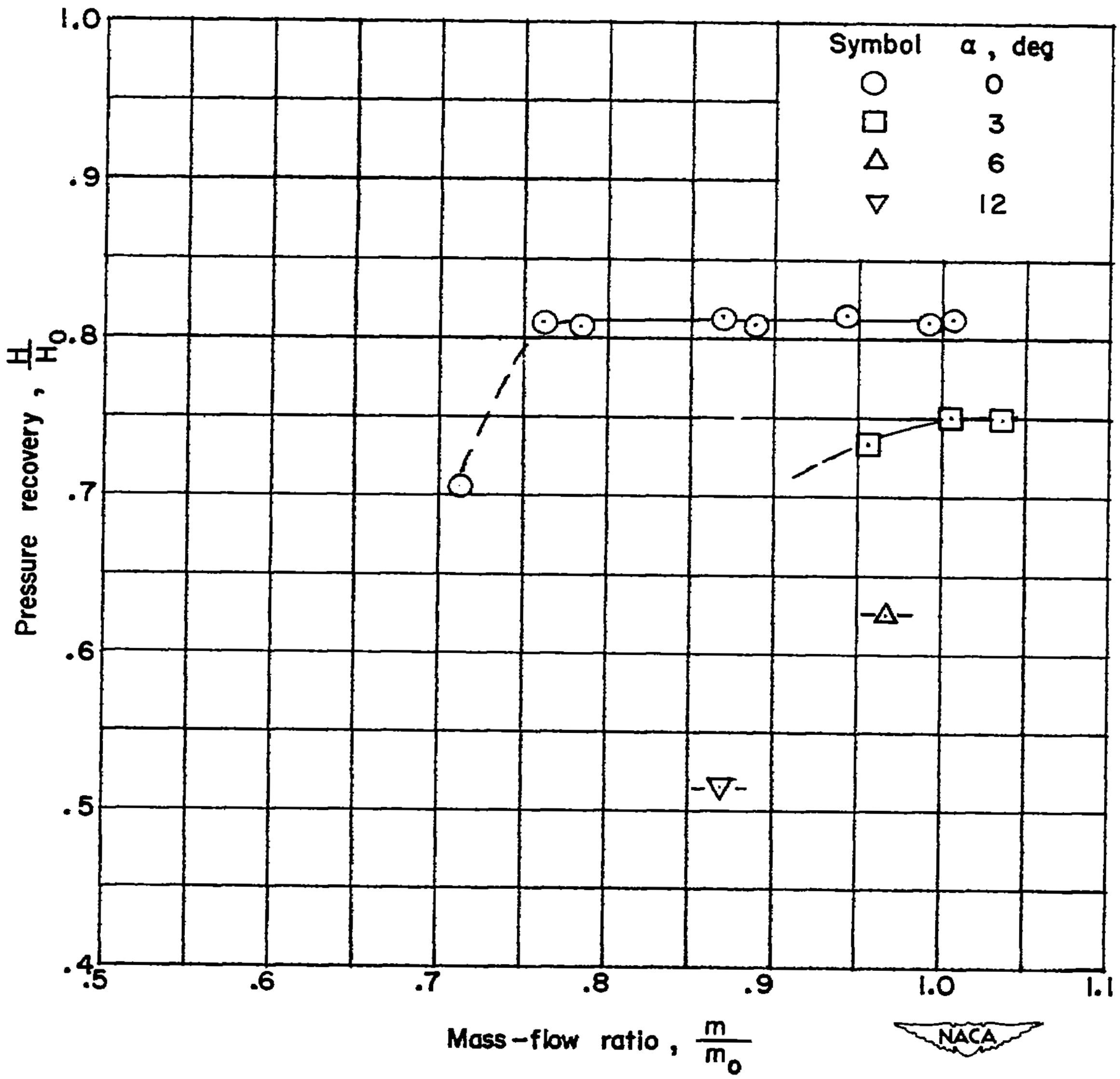

(a) $\phi = 0^{\circ}$.

Figure 12.- Variation of mass-flow-weighted mean total-pressure recovery with inlet mass-flow ratio for the design position of the central body. $\theta_L = 42.4^{\circ}$.

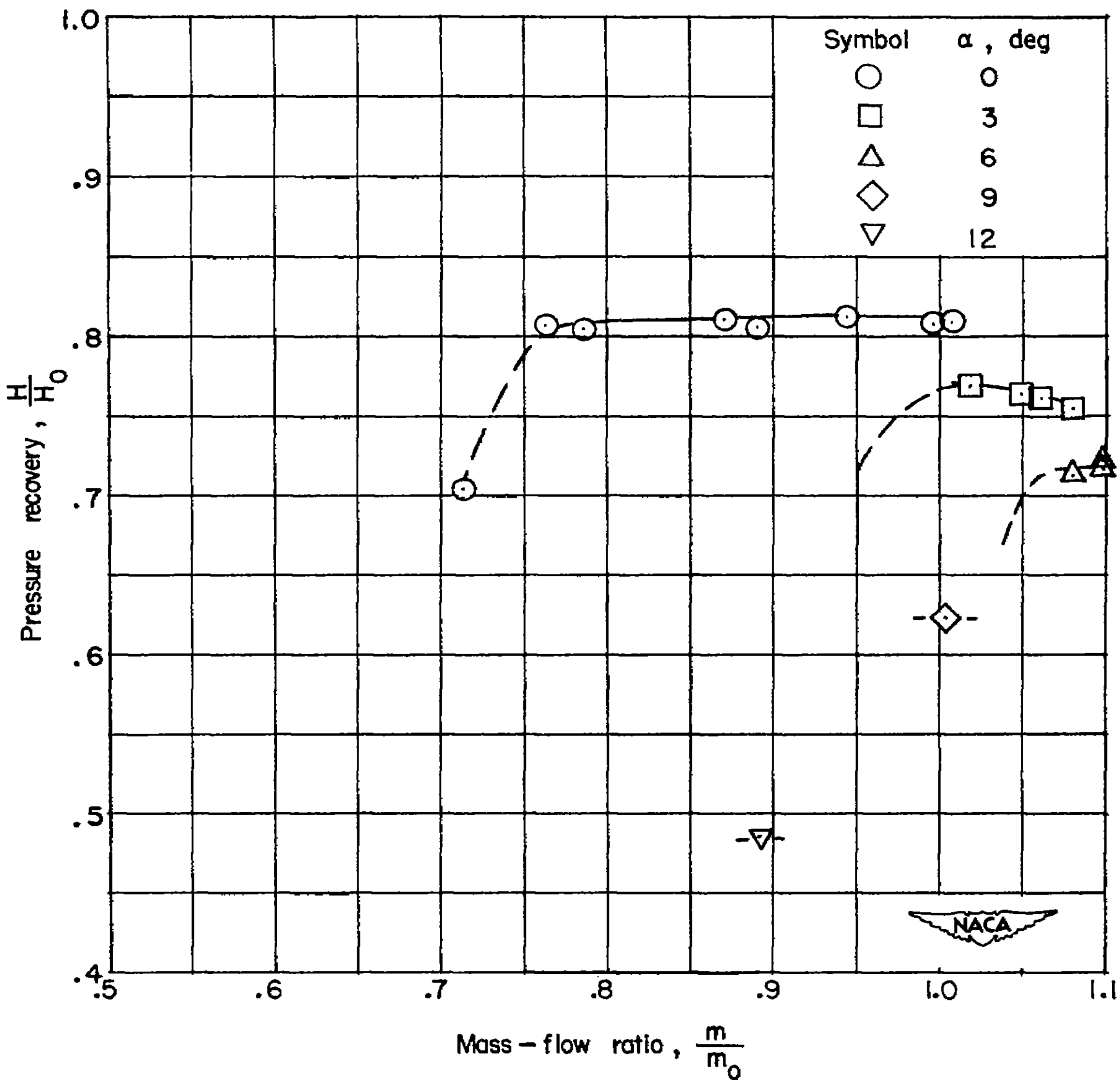

(b) $\phi = 45^{\circ}$.

Figure 12.- Continued.

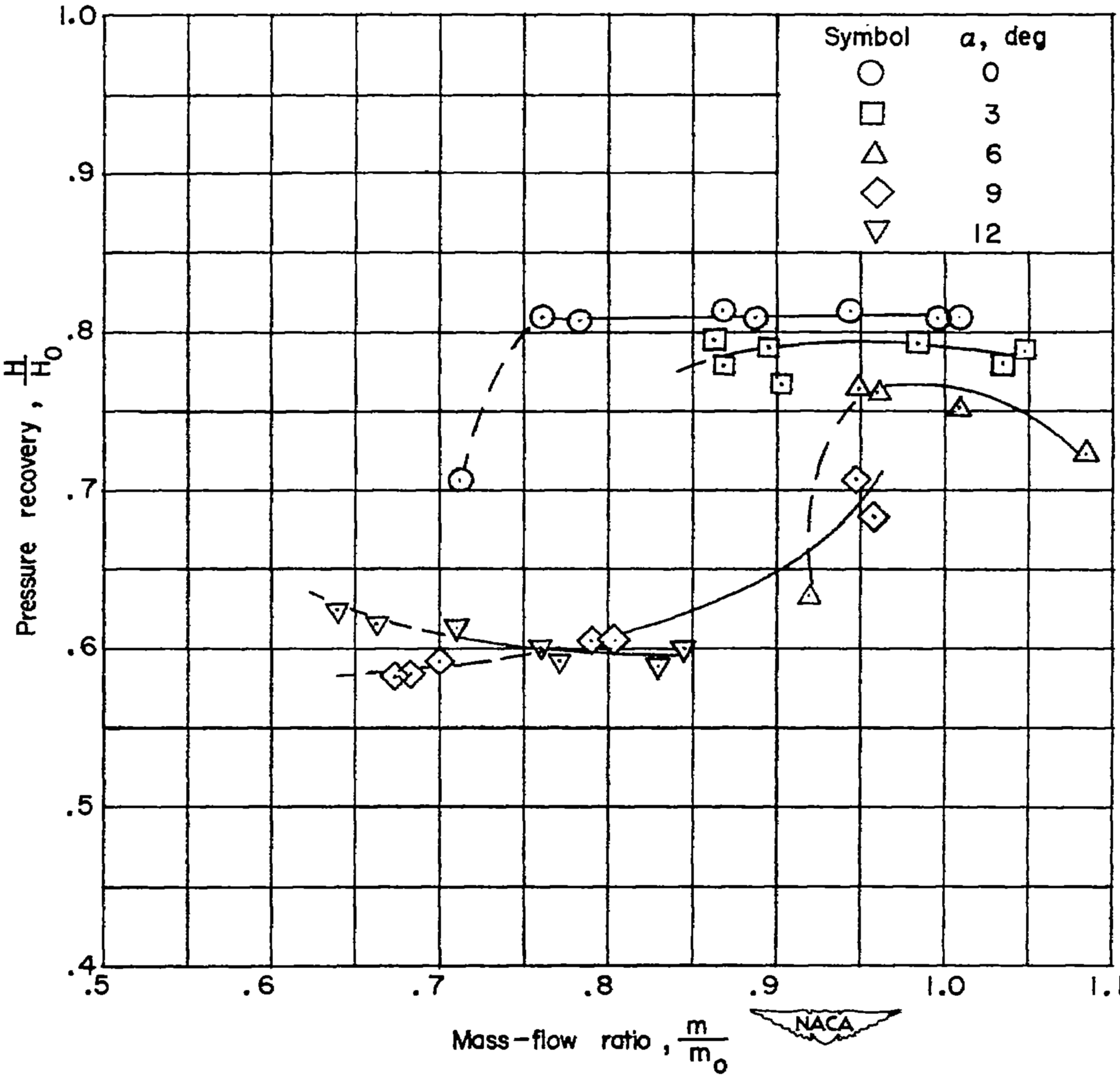

(c) $\phi = 90^\circ$.

Figure 12.- Continued.

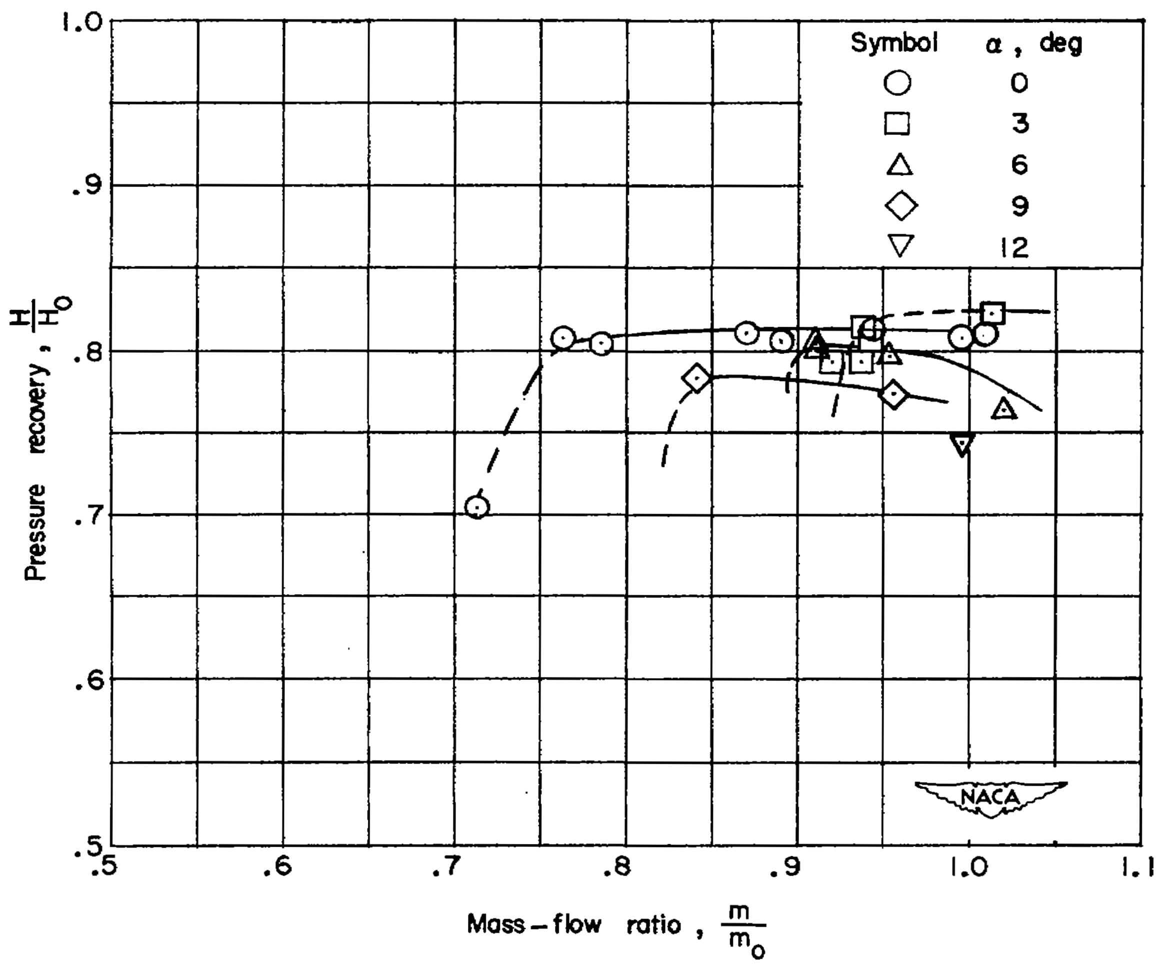

(d) $\phi = 135^{\circ}$.

Figure 12.- Continued.

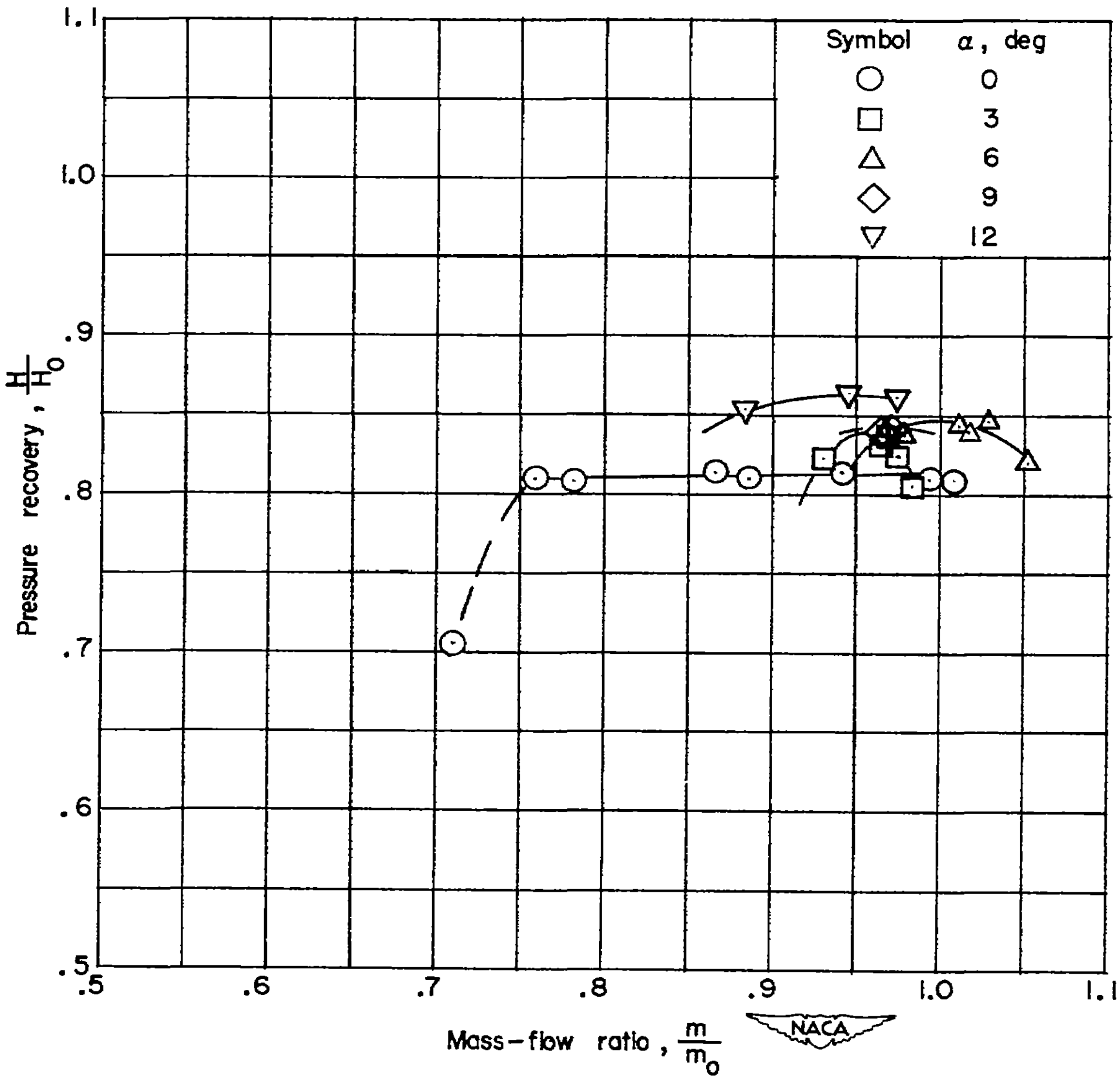

(e) $\phi = 180^{\circ}$.

Figure 12.- Concluded.

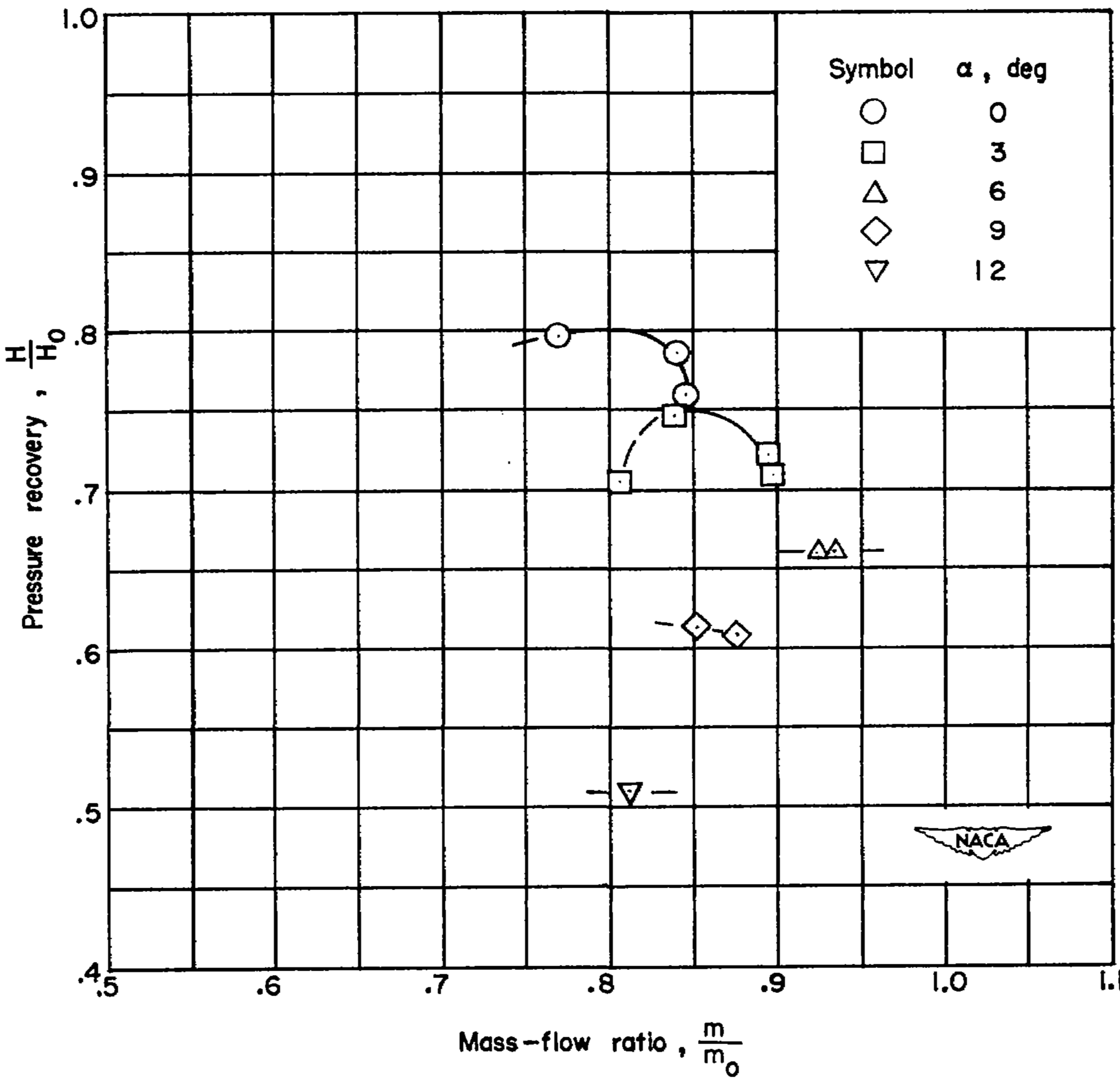

(a) $\phi = 0^{\circ}$.

Figure 13.- Variation of mass-flow-weighted mean total-pressure recovery with inlet mass-flow ratio for the off-design position of the central body. $\theta_L = 38.0^{\circ}$.

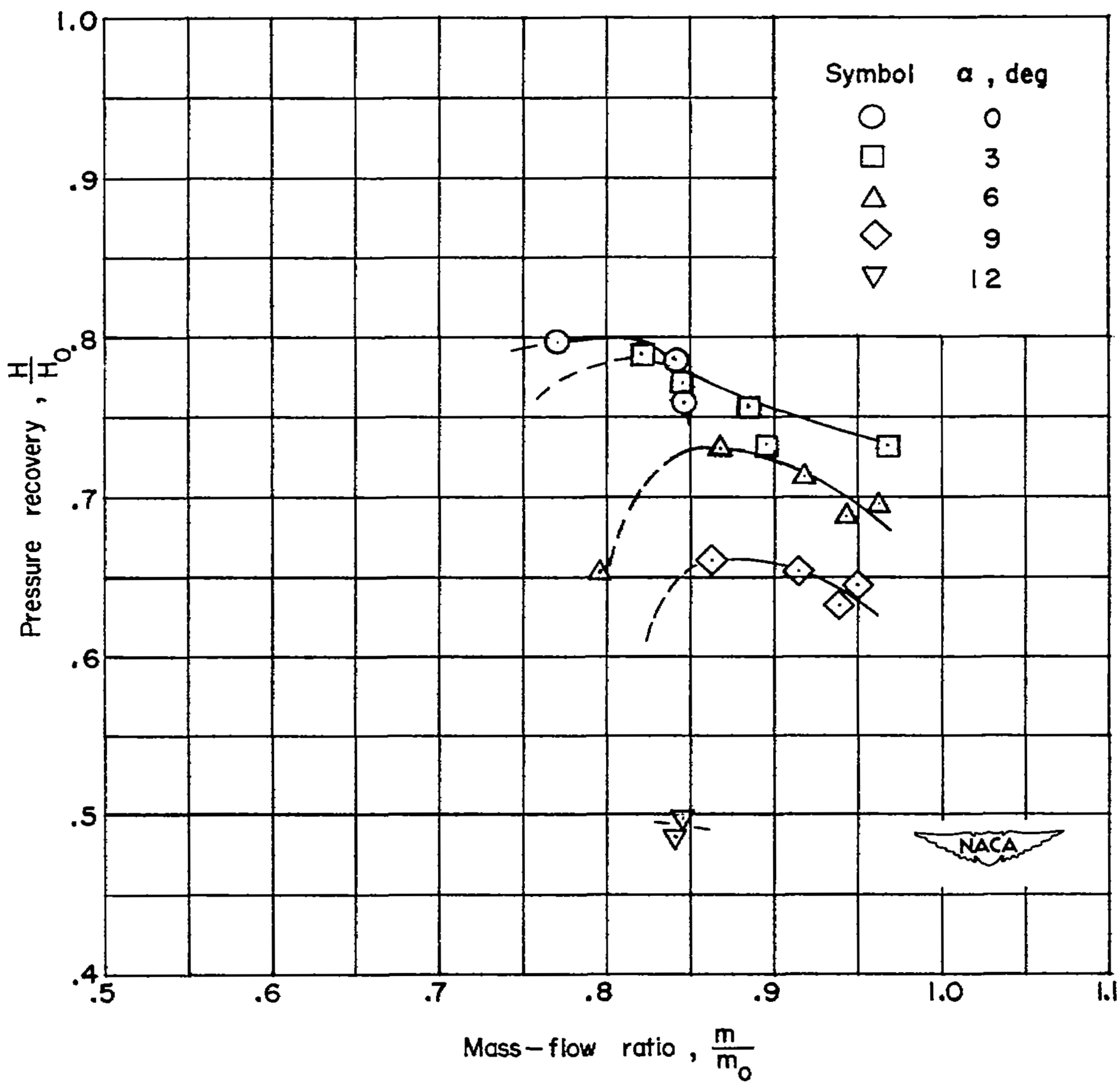

(b) $\phi = 45^\circ$.

Figure 13.- Continued.

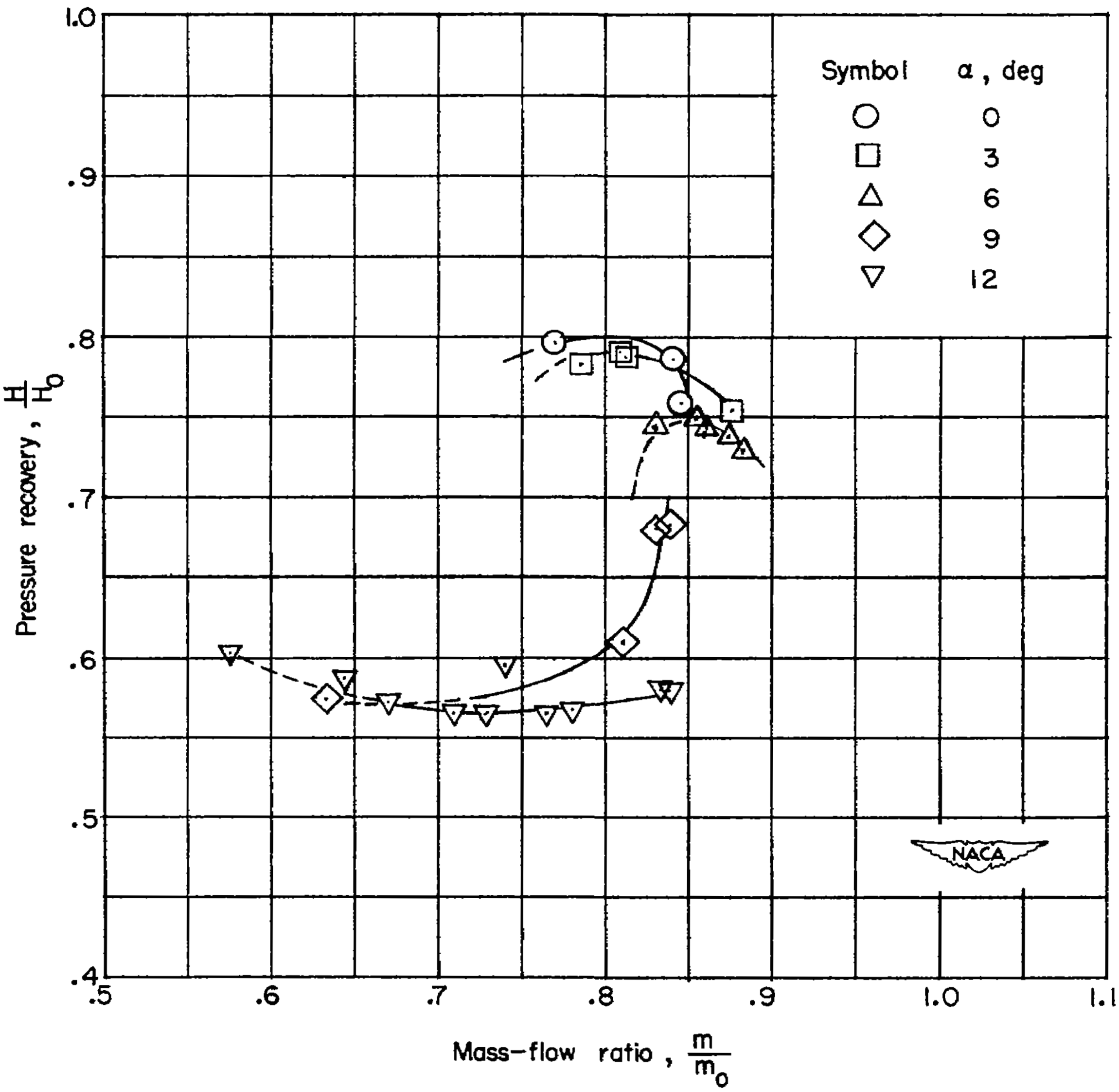

(c) $\phi = 90^{\circ}$.

Figure 13.- Continued.

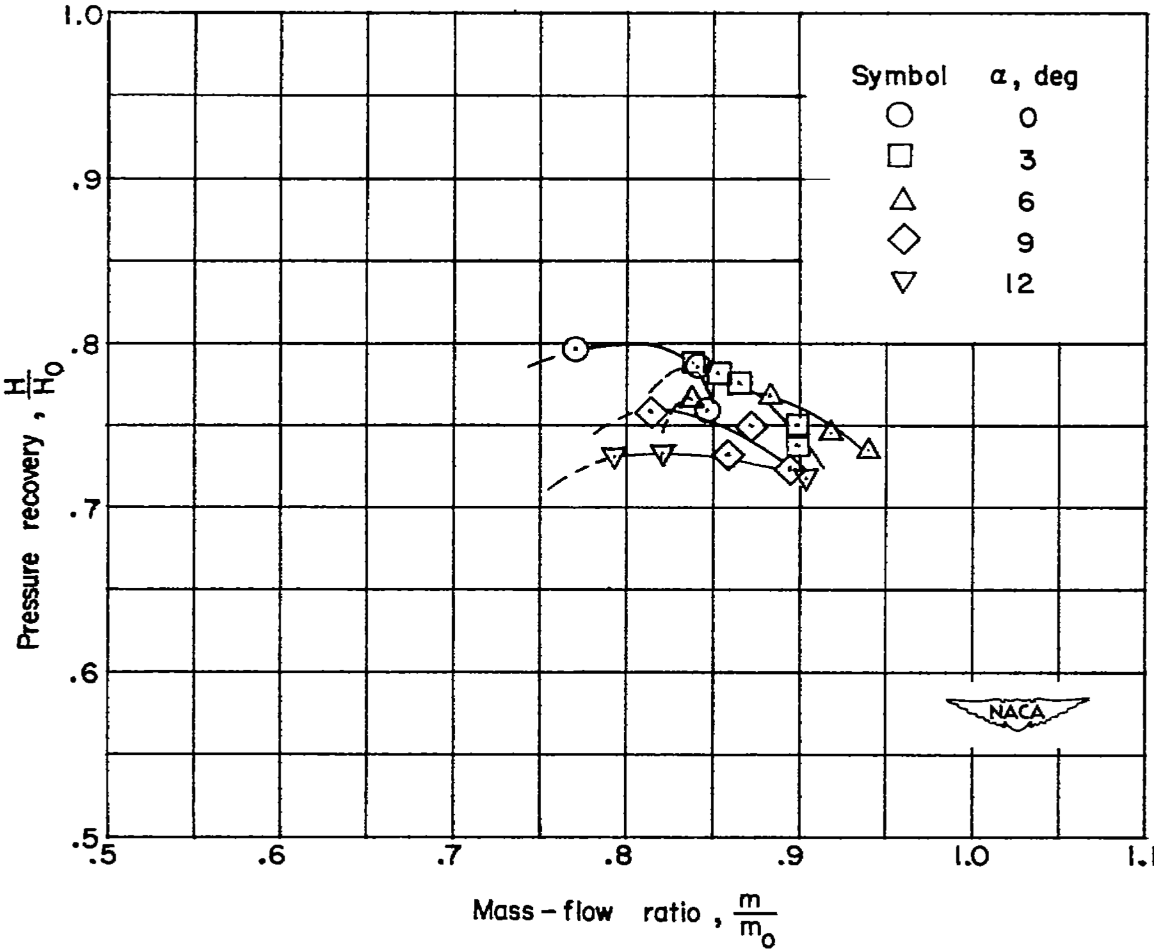

(d) $\phi = 135^{\circ}$.

Figure 13.- Continued.

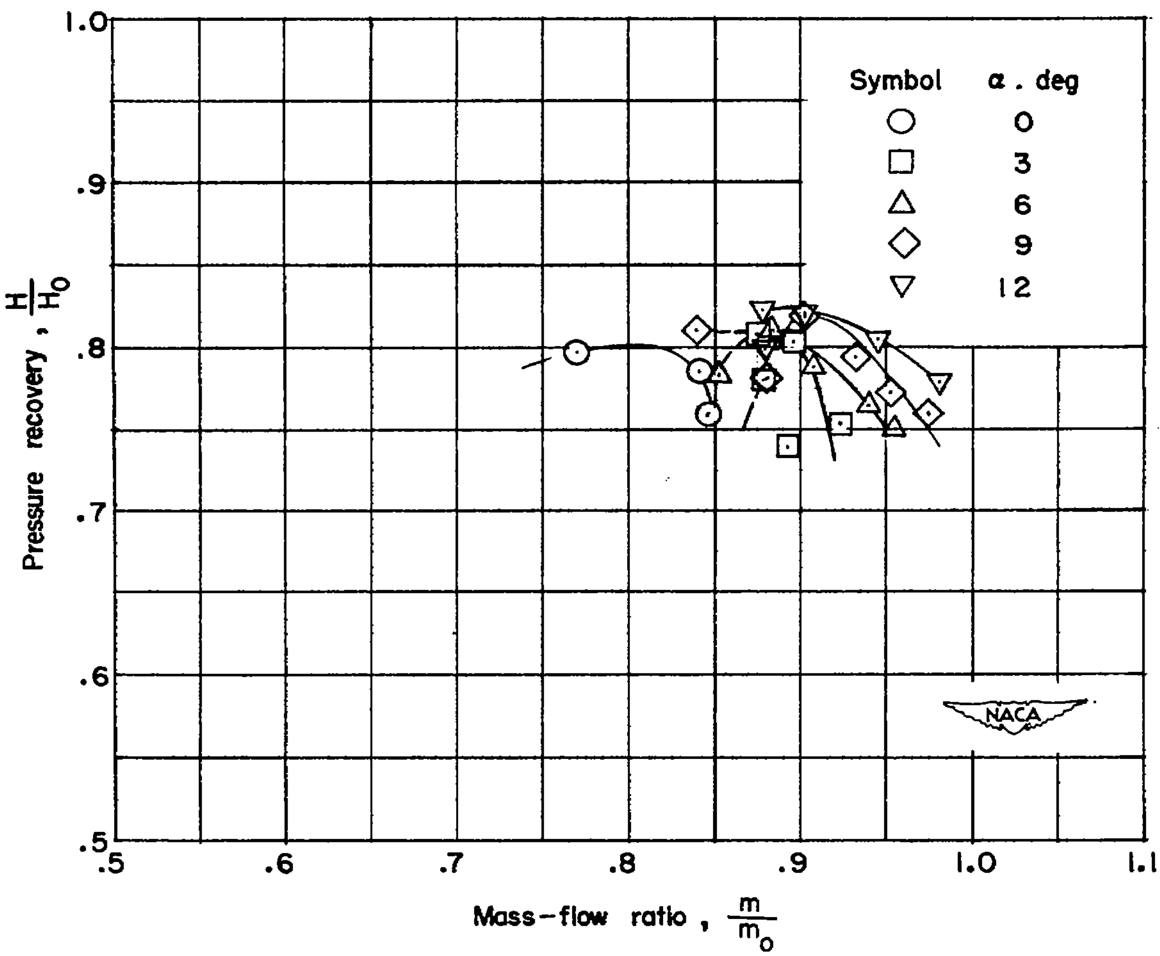

(e) $\phi = 180^{\circ}$.

Figure 13.- Concluded.

[redacted]

[redacted]

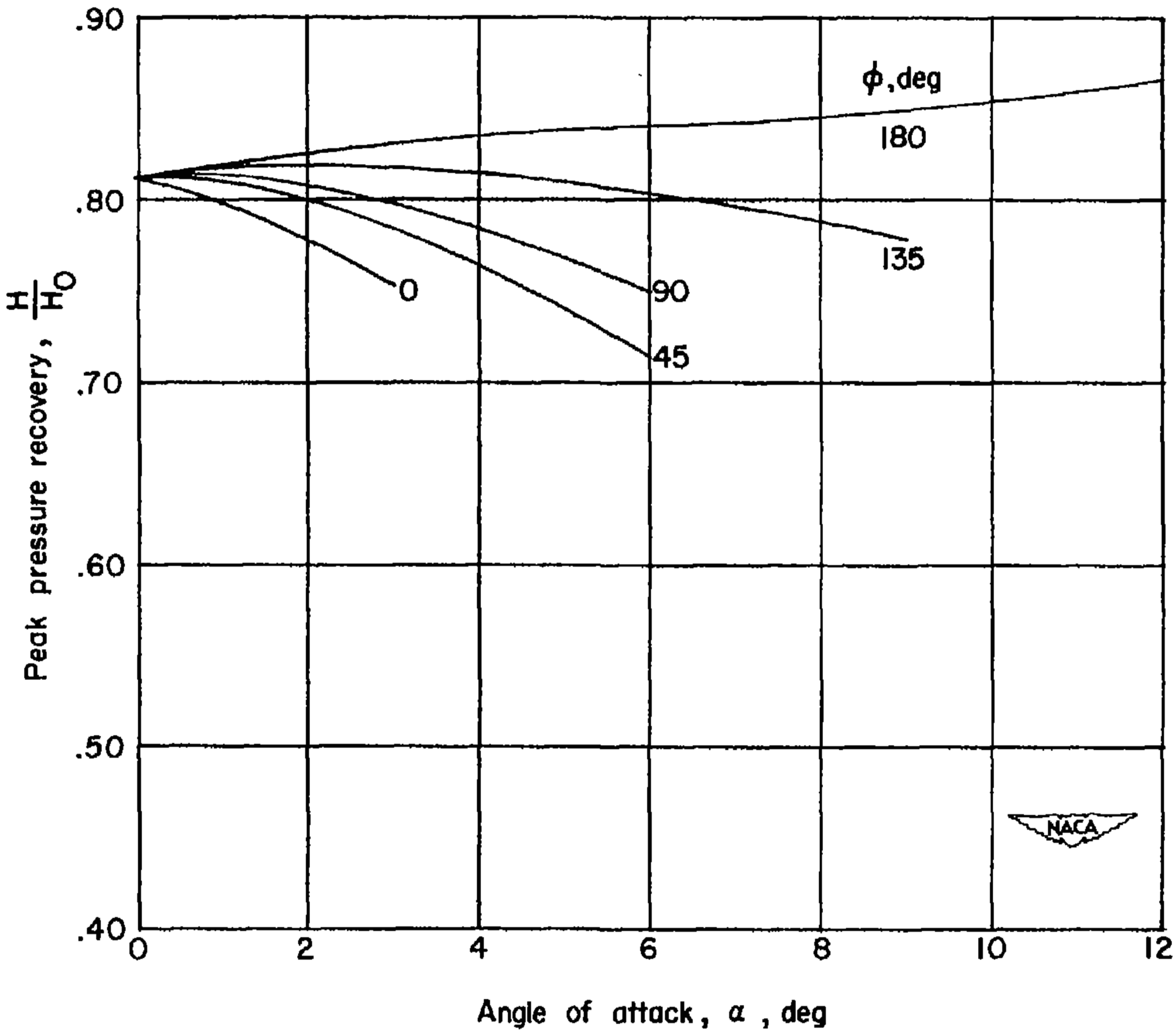

Figure 14.- Effect on peak inlet pressure recovery of circumferential location of inlet on fuselage. $\theta_L = 42.4^\circ$ (design condition).

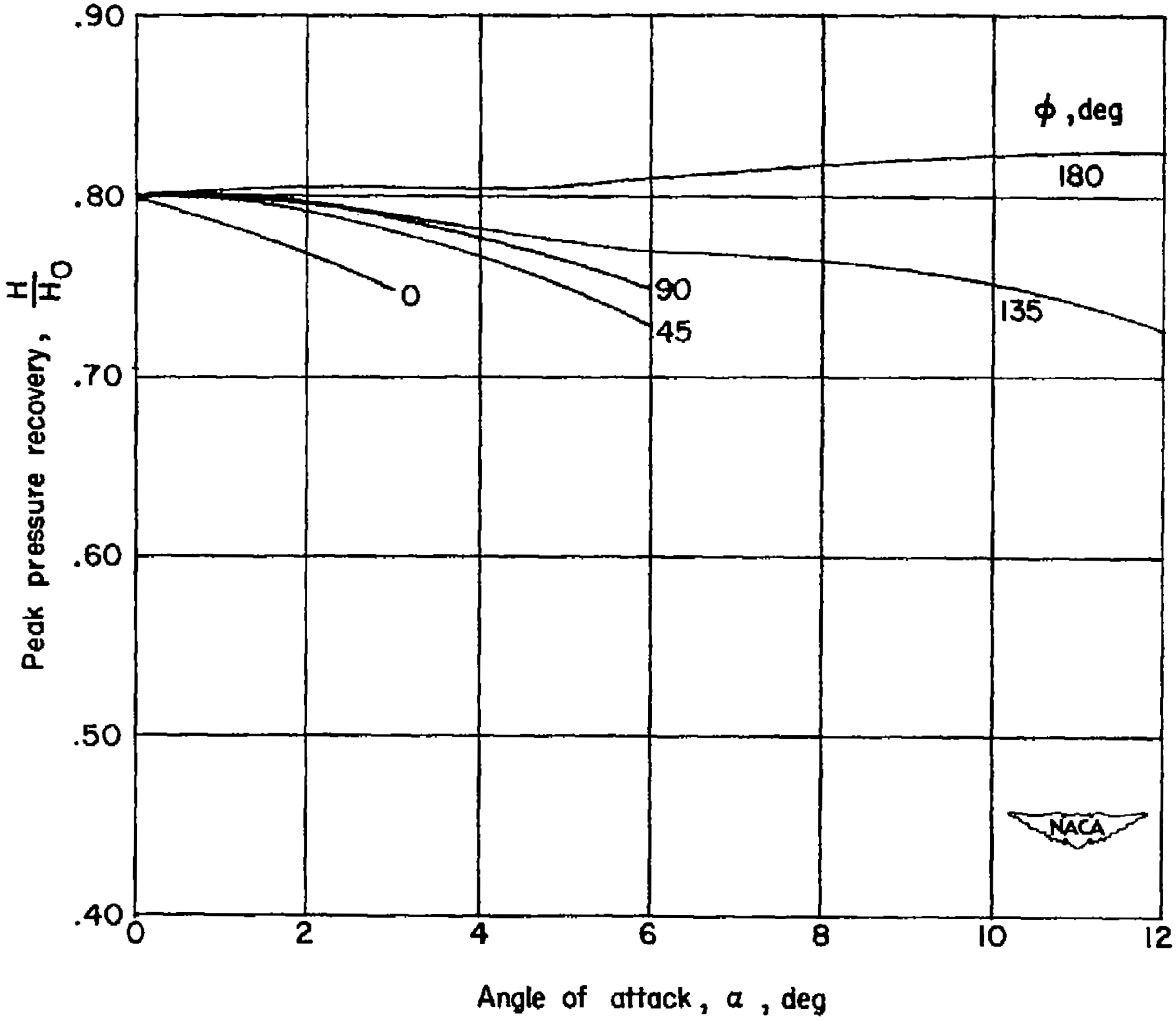

Figure 15.- Effect on peak inlet pressure recovery of circumferential location of inlet on fuselage. $\theta_L = 38.0^{\circ}$ (off-design condition).

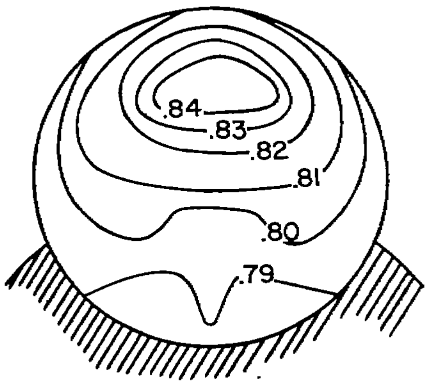

(a) $\alpha = 0°$; $\frac{m}{m_o} = .94$; $\frac{H}{H_o} = .81$

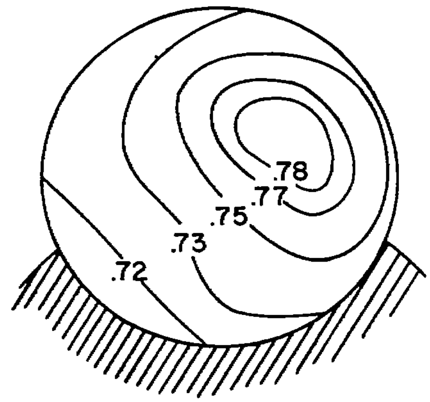

(b) $\alpha = 3°$; $\phi = 0°$; $\frac{m}{m_o} = 1.07$; $\frac{H}{H_o} = .76$

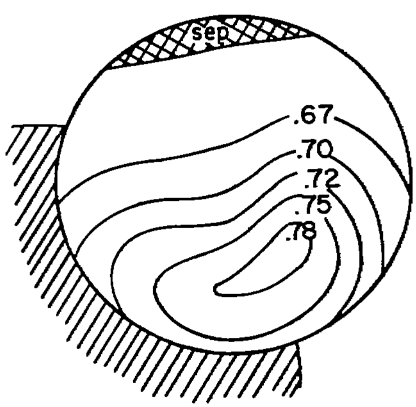

(c) $\alpha = 6°$; $\phi = 45°$; $\frac{m}{m_o} = 1.10$; $\frac{H}{H_o} = .72$

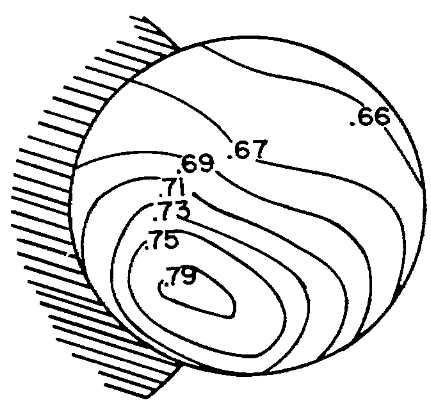

(d) $\alpha = 6°$; $\phi = 90°$; $\frac{m}{m_o} = 1.08$; $\frac{H}{H_o} = .72$

Figure 16.- Local total-pressure-recovery maps at diffuser station 36.94.

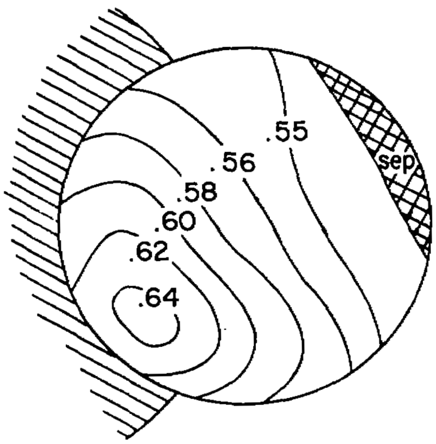

(e) $\alpha = 12°$; $\phi = 90°$; $\frac{m}{m_o} = .74$; $\frac{H}{H_o} = .60$

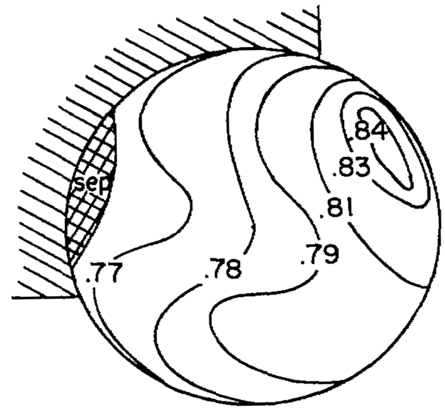

(f) $\alpha = 6°$; $\phi = 135°$; $\frac{m}{m_o} = .95$; $\frac{H}{H_o} = .80$

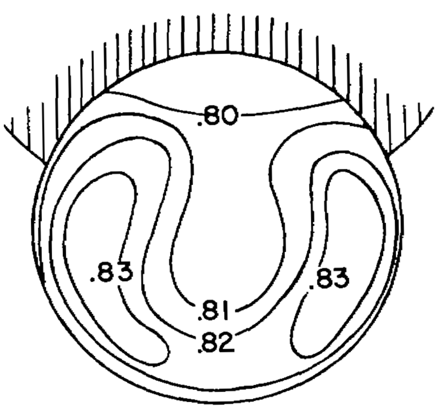

(g) $\alpha = 6°$; $\phi = 180°$; $\frac{m}{m_o} = 1.05$; $\frac{H}{H_o} = .82$

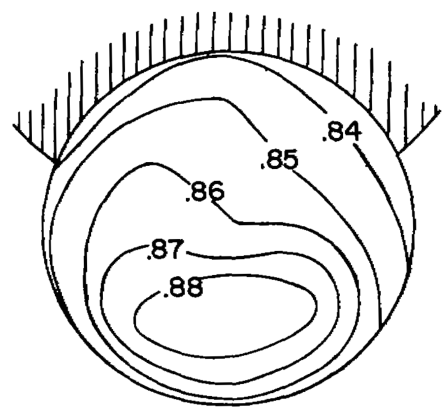

(h) $\alpha = 12°$; $\phi = 180°$; $\frac{m}{m_o} = .95$; $\frac{H}{H_o} = .86$

Figure 16.- Concluded.

[redacted]

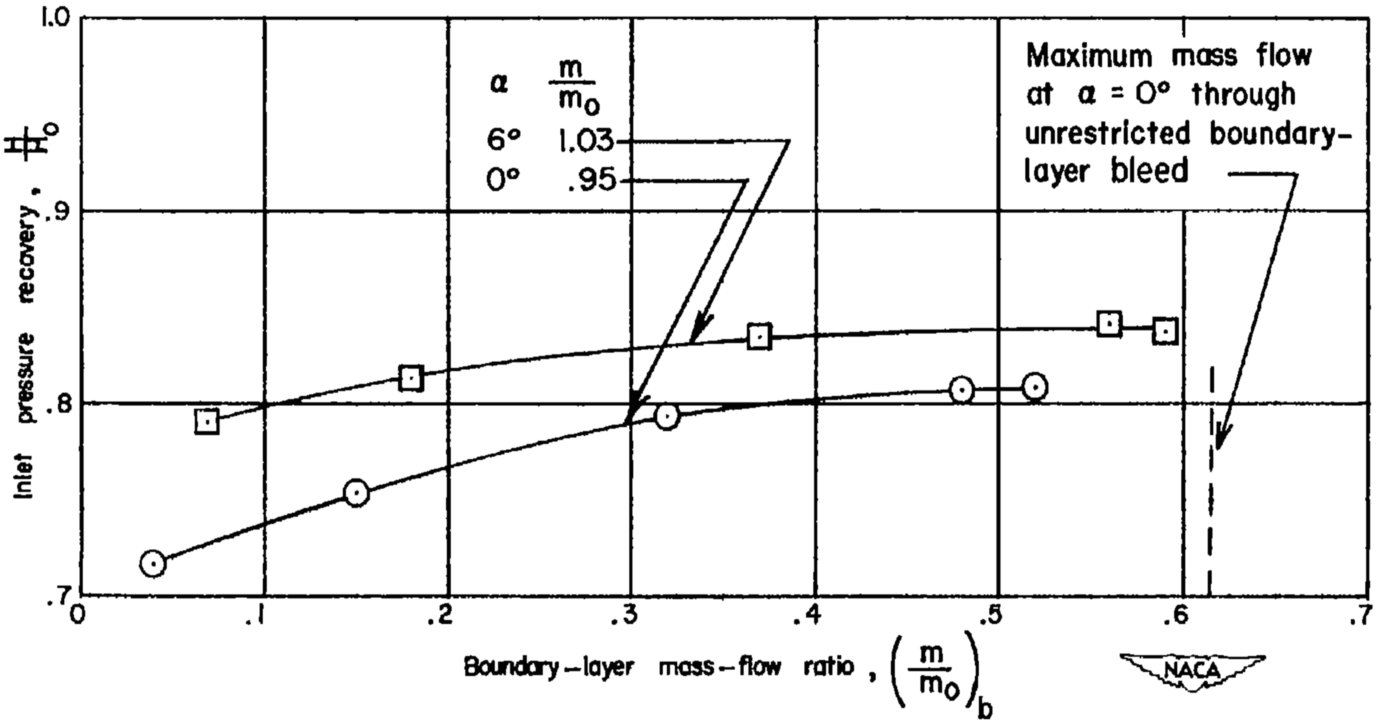

Figure 17.- Effect of boundary-layer-bleed mass-flow ratio on inlet pressure recovery. $\phi = 180^{\circ}$.

SECURITY INFORMATION

Restriction/Classification Cancelled

[redacted]

[redacted]